ALMA MATER STUDIORUM
UNIVERSITÀ DI BOLOGNA

DOTTORATO DI RICERCA IN

SCIENZE CHIRURGICHE

Ciclo 37

Settore Concorsuale: 06/D4 - MALATTIE CUTANEE, MALATTIE INFETTIVE E MALATTIE DELL'APPARATO DIGERENTE

Settore Scientifico Disciplinare: MED/35 - MALATTIE CUTANEE E VENEREE

MACHINE AIDED DIAGNOSIS AND MELANOMA: HISTOPATHOLOGICAL FINDINGS

Presentata da: Giulia Veronesi

Coordinatore Dottorato

Emanuela Marcelli

Supervisore

Emi Dika

Co-supervisore

Nico Curti

Esame finale anno 2025

Abstract

Introduction. The incidence of cutaneous melanoma has risen in recent years. Histopathological examination remains the gold standard for diagnosing cutaneous melanoma; however, it is often complex, with a discrepancy rate of 2.7–26% in identifying melanocytic neoplasms. The need to streamline workflows and develop new diagnostic support methods for cutaneous melanoma has driven increased research into the application of artificial intelligence. Our study is structured into three main sections: (i) automated silhouette definition and its diagnostic significance, (ii) extraction of nuclear features and classification modeling, and (iii) assessment of Breslow thickness.

Materials and Methods. This study was conducted in collaboration with the Department of Statistical Sciences (UNIBO), the Department of Physics and Astronomy (UNIBO), and the Oncologic Dermatology Unit at IRCCS Azienda Ospedaliero-Universitaria di Bologna, Italy. Digital whole slide images were acquired using a scanner at 40x magnification. An AI-based image processing pipeline was applied to each image to segment nuclear cells and delineate the tumoral area (silhouette). The geometric contours of nuclear cell shapes and their spatial distribution were analysed. A classification model using Linear Discriminant Analysis was implemented. Finally, AI models were applied to measure Breslow thickness.

Results. (i) The automated silhouette identified by our pipeline closely matches those manually contoured by expert dermatopathologists, and based on its morphological characteristics, pathologists were able to diagnose melanoma with an error rate of just 4%. (ii) The morphological features of 2,204,813 nuclei were evaluated, and each sample's characteristics were summarized using 44 variables. Classification accuracy, assessed through Monte Carlo Cross-Validation, achieved an accuracy of 0.90 and a sensitivity of 0.84 in distinguishing cutaneous melanoma. (iii) We noted variability in a distance measure and heterogeneity in its acquisition methods. By evaluating the overall spatial distribution of cells, we observed a significant correlation between the pathologist-annotated distances and the 80th percentile of the cell distribution.

Conclusion. Automating clinical procedures provides invaluable support, leading to faster and more reliable sample evaluations. Our study can expedite the screening of whole slide image by prioritizing histopathology slides that exhibit high-risk melanoma features over those with low-risk nevus characteristics.

Sommario

Introduction ... 3
H&E histological analysis ... 6
Lesion's silhouette ... 7
Epidermal pattern and presence of ulceration ... 8
Dermo-epidermal junction pattern ... 9
Spatial distribution of cells ... 9
Dermis alteration ... 10
Cytological atypia ... 12
Tumour Breslow Thickness ... 13
Second opinion review of pathology specimens ... 14
Immunohistochemical (IHC) ... 15
Artificial intelligence in histopatological melanoma diagnosis ... 17
Purpose of the Study ... 20
Automated silhouette definition and its diagnostic power ... 20
Material and Methods ... 20
Computer aided diagnosis system pipeline ... 21
Silhouette definition ... 21
Results ... 22
Discussion ... 25
Nuclei features extraction and classification model ... 27
Material and Methods ... 27
Nuclei Features Extraction ... 27
Classification Model ... 30
Results ... 31
Discussion ... 34
Evaluating Breslow thickness ... 36
Material and Methods ... 36
Results ... 37
Discussion ... 40
Conclusion ... 43
References ... 43

Introduction

Cutaneous melanoma (CM) is the deadliest form of skin cancer, with 57 000 deaths in 2020 (0·7% of all cancer deaths), according to the Global Cancer Observatory. [1,2]

The incidence of CM has been rising globally over the past few decades, particularly in countries with predominantly fair-skinned populations or those with excessive sun exposure due to closer proximity to the equator. [3]Age-cohort period analyses of melanoma incidence conducted between 1982 and 2011 in Australia, New Zealand, Norway, Sweden, the UK, and the white population of the USA revealed an approximate annual increase of 3%, with this upward trend continuing in subsequent years.[4] In Europe, the incidence rate is 10 to 25 new CM cases per 100'000 inhabitants, with a significant increase among individuals over 60, particularly men. The primary risk factors include UV exposure, especially intermittent high sun exposure leading to sunburn, a high number of common nevi, large congenital nevi (CN) or atypical/dysplastic nevi (DN), and genetic predisposition. [5]

It is important to note that the incidence and mortality rates of CM vary globally depending on the quality and accessibility of primary care, availability of early diagnosis, effectiveness of primary prevention and advancements in disease management. In the clinical setting, the diagnosis of melanoma can vary significantly based on the level of medical training, expertise, and access to new technologies.

A standard measure for melanoma detection is the number needed to biopsy (NNB), which indicates how many skin biopsies are performed to detect one case of melanoma. The NNB for melanoma ranges from 4 to 26 The use of dermoscopy, digital dermoscopy, sequential total body photography, and reflectance confocal microscopy has been shown to directly improve diagnostic accuracy in detecting melanoma. [5–7] (Fig.1-3)

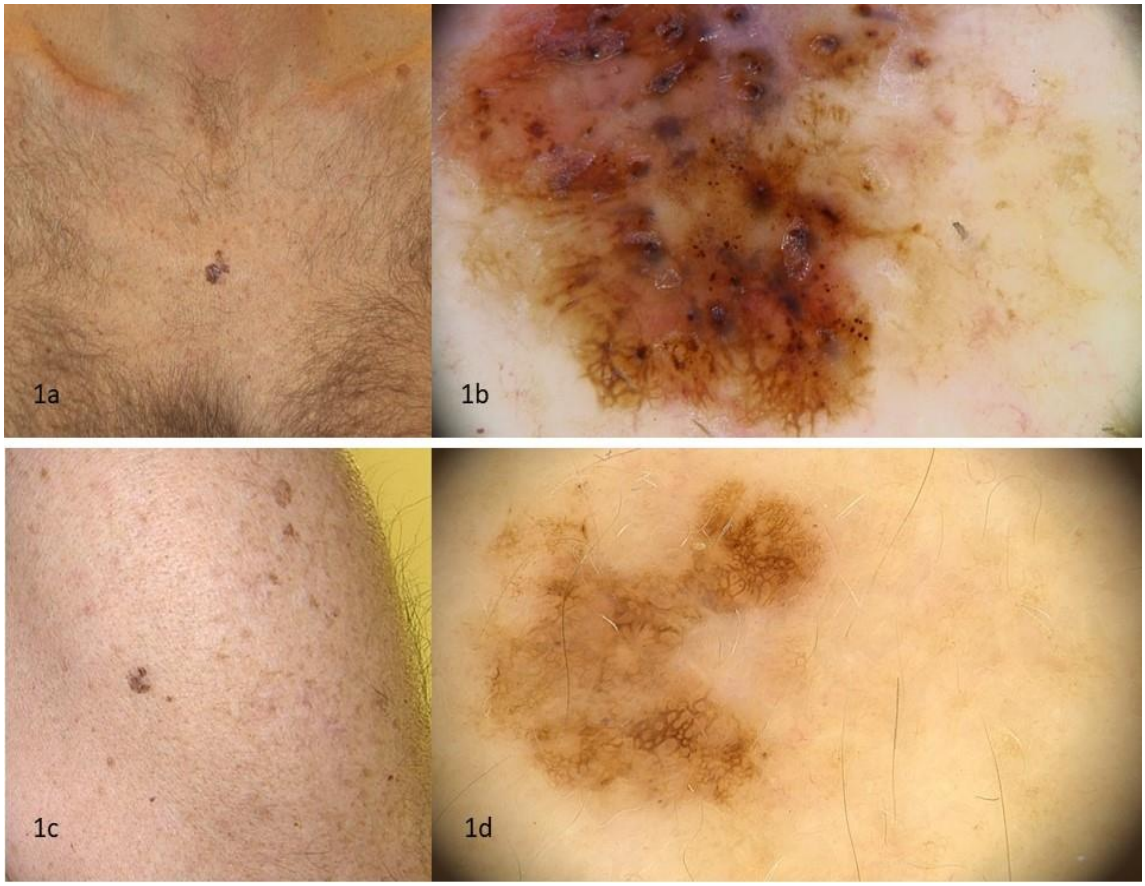

Figure1- Two examples of superficial spreading CM. Clinically, both presented as pigmented macules with irregular borders (1a, 1c). Dermoscopically, they show streaks and whitish, structureless regression features, more pronounced in the first case (1b), representing a 0.5 mm melanoma according to tumor Breslow thickness, and more subtle in the second case (1d), representing a 0.2 mm melanoma according to tumor Breslow thickness.

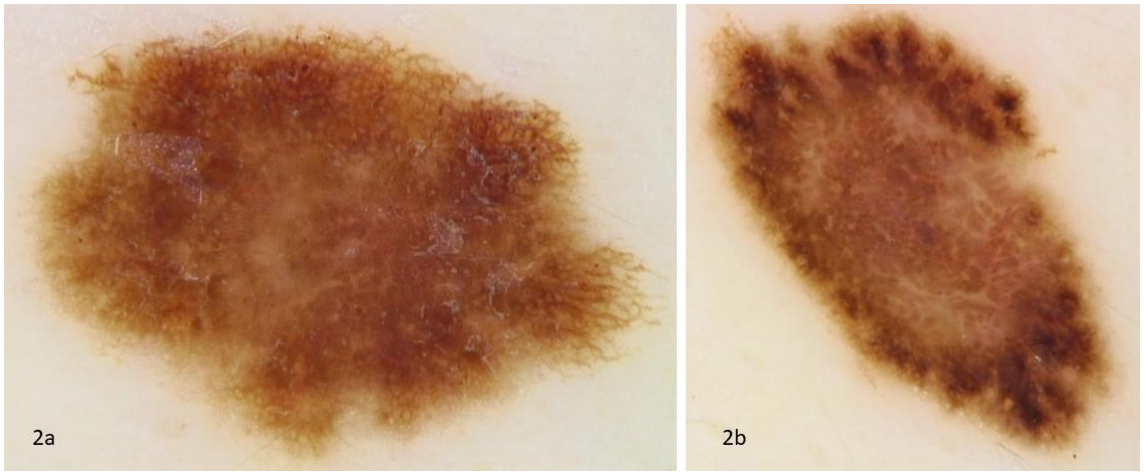

Figure 2- Dermoscopy is important as it allows for differential diagnosis between lesions that are difficult to recognize or appear similar. Here, we have two seemingly similar lesions, both displaying an irregular network: a DN (2a) and a CM (2b). In the latter case (2b), we observe how the network reverses in the central portion, creating a white mesh pattern typical of one of the dermoscopic criteria for melanoma

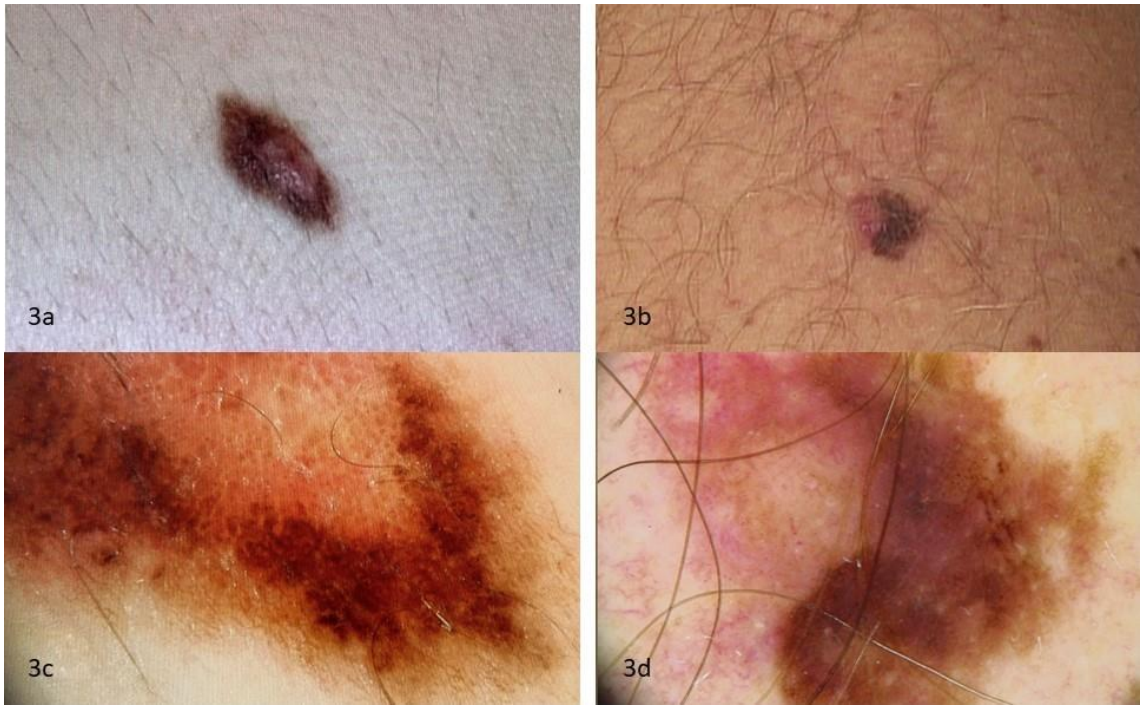

Figure 3- Two more similar cases. Clinically, both have a worrisome appearance, with multiple colors and irregular borders (3a, 3b). Dermoscopically, one shows a combined pattern with a central dermal component lacking atypical vascularization and a regular peripheral network, indicating a dermal nevus with junctional activity (3c). The other, however, displays a combined pattern with a dermal component featuring polymorphous vascularization and an irregular peripheral network, indicating a melanoma arising from a nevus (3d).

The gold standard for diagnosing CM is the histopathological examination of haematoxylin and eosin (H&E)-stained tissue biopsy sections analysed via light microscope.[8,9] This allows pathologists to observe the disease at the cellular level and apply their expertise to assess the tissue's morphological and cytological features for accurate diagnosis. However, manual evaluation of tissue samples is often complex, making it a time-consuming and labour-intensive process. Additionally, the high volume of skin biopsies in most pathology laboratories presents significant logistical and staffing challenges. Interpretation and classification of histological specimens rely on integrating various histological features, which may be influenced by the pathologist's subjectivity. As a result, diagnostic discrepancies for melanocytic neoplasms have been reported to range from 2.7% to as high as 25%–26%. [10–12] A worrying study, demonstrated an interobserver variation in diagnostic sensitivity among 20 pathologists ranging from 55% to 100%, making the results almost as unpredictable as a coin toss.[13]

The most common issues with inter- and intra-observer variability among pathologists involve the diagnosis of small or flat lesions, as well as lesions with spitzoid morphology. [11–16] Terms with uncertain prognoses, such as atypical Spitz tumour (AST) and superficial atypical melanocytic proliferation of uncertain malignant significance (SAMPUS) have been suggested by the medical community and introduced into daily practice. [17] In particular, there is a tendency to overdiagnosis thin melanomas due to the difficulty in distinguishing between junctional-type DN and in situ/superficial spreading CM. [18–20]

For these types of lesions, it is important to implement new methods to aid in differential diagnosis. [21]

H&E histological analysis

In the late 1940s, Ackerman was among the first to systematically describe the pathology of what was then referred to as "melanocarcinoma".[22] At that time, it was widely believed that all melanomas originated from preexisting moles, particularly the so-called "active junctional nevus".[23] From a modern perspective, much of what was once considered a precursor lesion would likely now be classified as melanoma in situ. Ackerman, along with Allen, Spitz, and Clark, were pioneering figures in the field of melanoma pathology. Many of the histopathologic criteria for diagnosing melanoma, which are still widely used by dermatopathologists today, were established in the 1970s. Around the same time, Breslow introduced depth of invasion as a prognostic marker for primary cutaneous melanoma.[24] Ackerman, however, rejected the concept of precursor lesions such as "active junctional nevus", "dysplastic lentiginous nevus of the elderly" and "premalignant melanosis" considering them to be misdiagnoses of melanoma in situ. [16]

The histopathologist's diagnosis relies on visually assessing the overall architectural pattern (morphological features) and various cellular characteristics (cytological features) in histological samples.[25] This process involves multiple steps of analysis and reasoning, which are essential for determining whether a neoplasm is benign or malignant.

Morphological features are examined under low microscopic magnification (2x to10x), while cytological features identifying cellular atypia are observed at high microscopic magnifications (20x to 100x)

Lesion's silhouette

One of the most crucial distinguishing features of a melanocytic neoplasm is its silhouette. [26] This term, introduced by Ackerman in 1985, describes the contour of the neoplasm and the morphologic aspects of tumour extension. [26] The importance of silhouette delineation, at a first glance, could be superior to that of other cytological details in determining the benign or malignant nature of a neoplasm. [26,27]

A neoplasm with a silhouette that is symmetrical, wedge-shaped, and sharply circumscribed with smooth borders is typically benign. In contrast, a silhouette that is asymmetrical, poorly circumscribed, and jagged in outline is almost always indicative of a malignant neoplasm. [25–27] The symmetry of the silhouette can be assessed in several ways:

- **Vertical symmetry**: This can be evaluated by drawing an imaginary vertical line through the centre of the lesion. If the two resulting halves are similar, the lesion is likely benign (Fig.4). [27]
- **Symmetry of lateral edges**: This refers to the features of the lesion's borders. A similar cellular arrangement and consistent cytological details on both sides are indicative of a benign lesion. [27]
- **Horizontal symmetry**: This can be assessed by dividing the lesion into several imaginary parallel strips. A benign nevus will show homogeneous histological details at each level of thickness, with uniform cellular characteristics and density. [27]

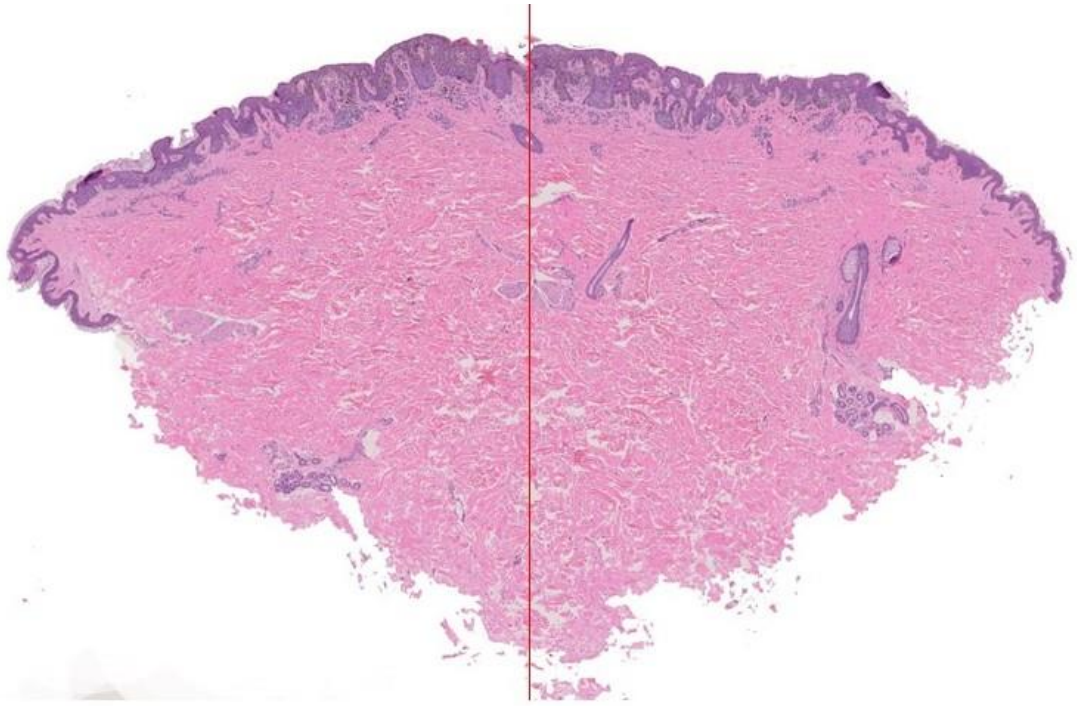

Figure 4- Vertical symmetry evaluated by drawing an imaginary vertical line through the center of the lesion. In this case of melanoma, we observe asymmetry between the two halves, particularly evident in the irregular distribution of nests, melanocytes at the junction, and the presence of skip areas—regions lacking cells alternating with areas where the cells are crowded together

Epidermal pattern and presence of ulceration

The evaluation of the epidermal pattern in nevi reveals uniform epidermal hyperplasia, with possible elongation or thickening of reticular ridges.[27] In contrast, melanoma typically exhibits a disordered pattern, or even ulceration (Fig.5). [27] Areas of epidermal hyperplasia are alternate with regions of epidermal thinning, leading to attenuation of the basal and suprabasal layers and loss of reticular ridges. [27] The consumption of epidermis and the presence of a linear dermo-epidermal artefactual cleft are both considered a good clue to melanoma. [9]

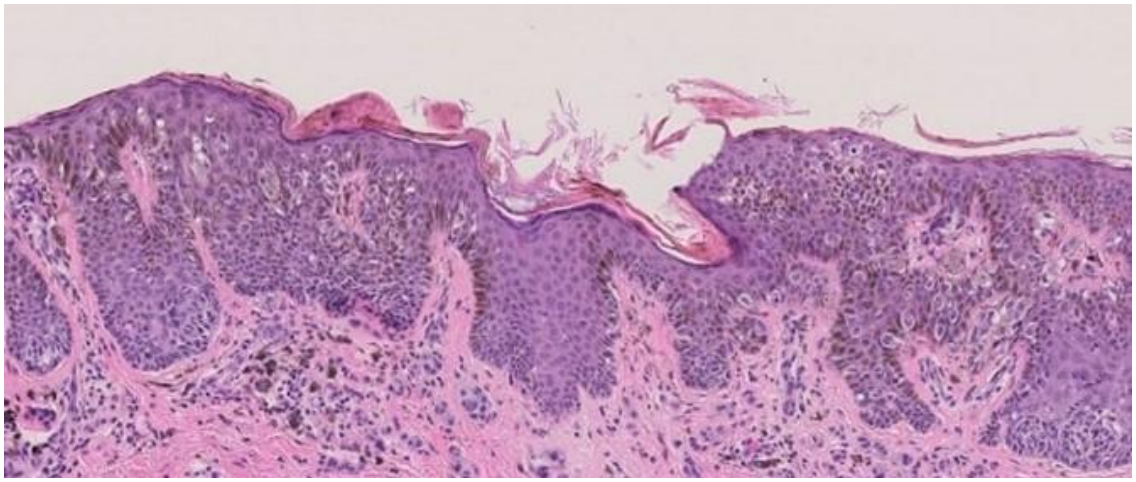

Figure 5- Ulcerated melanoma with the loss of an intact epidermis overlying the melanoma lesion.

Dermo-epidermal junction pattern

In melanoma, particular in superficial spreading type, the major disorder is localized on the dermo-epidermal junction (Fig. 6). [25] The nests in melanoma are large, confluent, irregularly shaped, and asymmetrically distributed at the junction. [25] They alternate irregularly with areas of single melanocytes or skip areas that are free of melanocytes. In nevi the nests are small and distributed without skip areas. Only Clark nevi could have variably sized or confluent nests .[25]

Spatial distribution of cells

In melanomas, single melanocytes are mostly irregularly distributed, not equidistant from one another, in both the basal layer and other epidermal layers, often within effaced rete ridges.[25,27] In contrast, in nevi, single melanocytes are typically observed in a lentiginous pattern, arranged as junctional single units within elongated rete ridges. [25,27]

Neoplastic cells can scatter into the epidermis and follicular epithelium, a process known as pagetoid spread, due to its resemblance to the scattering of breast cancer cells into the epidermis in Paget disease of the nipple or other sites.[25] This evaluation is particularly important for melanoma diagnosis, when numerous suprabasal melanocytes are involved, affecting the epidermal layers in a multifocal or diffuse manner, typically observed in both the central and peripheral portions of the lesion, and the melanocytes appear

atypical.[28] However, pagetoid spread can also occur in certain nevi. In nevi, the number of suprabasal melanocytes is generally low, limited to the spinous layer, and the phenomenon is focal or spatially restricted, usually occurring in the central portion of the lesion. This benign occurrence is referred to as pseudoinfiltration. [25]

Miescher also highlights that while the tendency of cells to separate or loosen from neighboring cells is a normal occurrence in benign nevi, it becomes much more pronounced in malignant melanoma.[29] A mild degree of disjunction can be observed in some compound junctional nevi, but the separation of individual cells is not as pronounced or widespread as in malignant melanomas. [25]

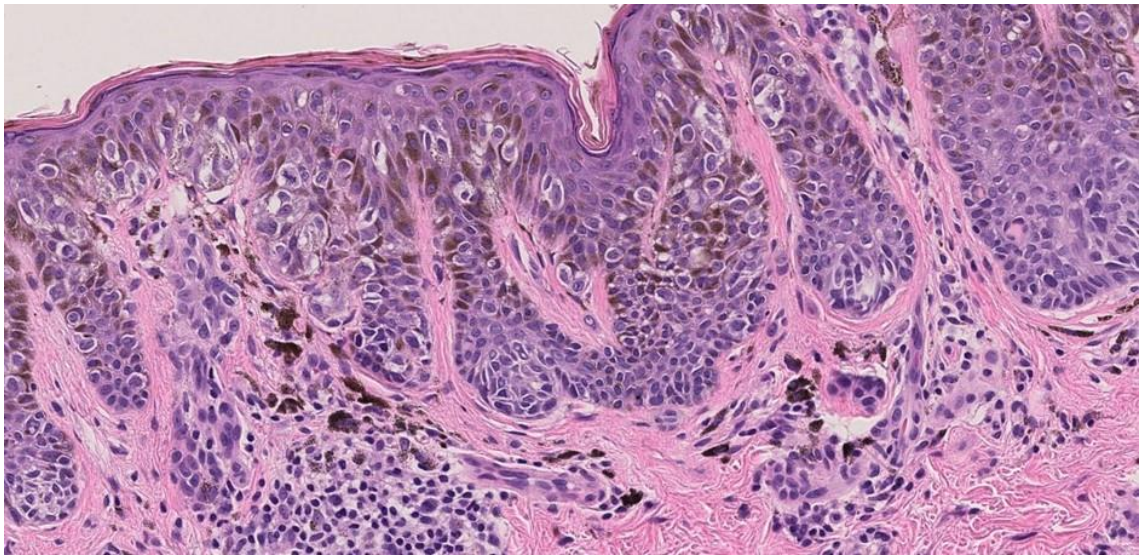

Figure 6 - At the junction, the atypical lesional cells are clustered in nests, but mostly are predominantly arranged as single units above the dermal papillae in a chaotic manner. The presence of pagetoid spread further supports the diagnosis of melanoma

Dermis alteration

The presence of atypical melanocytes in the dermis varies greatly basin on the melanoma subtypes.[28] The involvement of adnexal structures, vessels or nerves is an indication of a more aggressive clinical evolution. [30] a lymphocytic infiltrate with pigment incontinence and diffuse fibroplasia are frequently present in the papillary dermis. [28]

A dermal lymphocytic infiltrate, defined as present when evident beneath and/or within the context of melanocytic proliferation, may have either a sparse or pronounced distribution, sometimes forming a continuous band in the dermis. [28] An assessment of tumour-infiltrating lymphocytes (TIL) is critically important in the context of melanoma. In fact, studies have shown that the presence of intratumoral lymphocytes is generally a positive prognostic factor. [31,32]

The atypical melanocytes and TILs may alternate with diffuse fibroplasia (Fig.7) and areas of lesional cell loss, consistent with partial (or sometimes complete) regression.[15] The College of American Pathologists (CAP) defines histologic regression in melanoma as the replacement of tumour cells by lymphocytic inflammation, thinning of the epidermis, dermal fibrosis with inflammatory cells, melanophages, and telangiectasia.[33] Regression can be partial or complete. In partial regression, some melanoma cells remain surrounding or within the area of fibrosis, while in complete regression, no tumour cells are present.[34] Less than 0.27% of cases show complete regression, diagnosed by the absence of melanoma cells but evidence of fibrosis, melanophages, or a documented prior clinical lesion or the presence of metastatic disease. [34] In such cases, "tumorous melanosis" may appear, consisting of melanin-laden macrophages without melanocytes.[34]

Solar elastosis, which is seen in most cases of CM, consists of ribbon-like basophilic fibers, an abnormal product of damaged fibroblasts, typically found in sun-damaged skin.[34] The presence of solar elastosis beneath a melanocytic proliferation supports a melanoma diagnosis, particularly when the melanocytes seem to be pushing downward and are accompanied by fibrosis between them. [25]

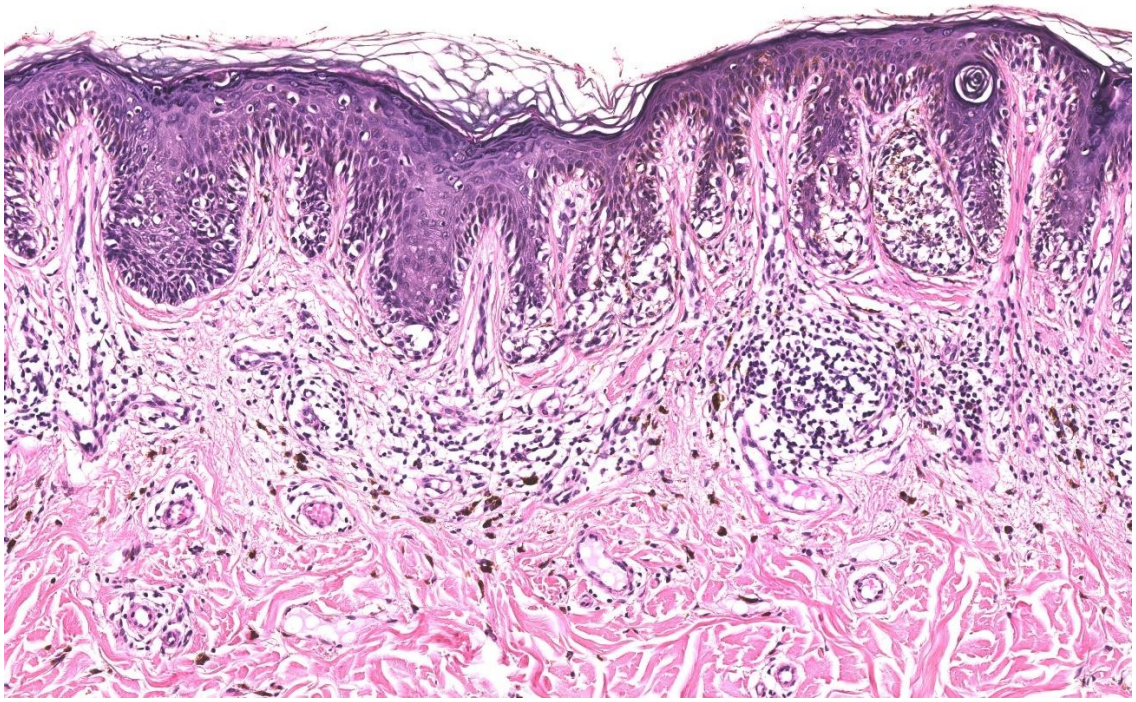

Figure 7: Lamellar fibroplasia presented as bands of pink collagen wrap around the rete and nests of melanocytes that bridge between them.

Cytological atypia

Atypical melanocytes show two basic traits. They may be large with abundant cytoplasm and a large nucleus, or small with scant cytoplasm and a hyperchromatic, angulated nucleus. As a result, cells and their nuclei can vary significantly in size and shape at the same level of the lesion. [25]

Despite some exceptions, nuclear pleomorphism, hyperchromasia, large eosinophilic nucleoli, and an irregular, thick nuclear contour are reassuring indicators of atypical melanocytes. Furthermore, necrosis and mitoses, specially in cluster or in the deep portion of the lesion are findings favouring a melanoma diagnosis (Fig.8). [25]

Cytological atypia, generally continuous and severe in melanomas, was discontinuous (atypical cells were mixed to nonatypical ones) and slight/moderate in naevi.[28] A practical method for assessing cytological symmetry is to draw parallel horizontal lines across the lesion. [25] In melanoma, the cytological details within each strip will vary, whereas in a nevus, the same cytological pattern is consistent throughout the entire section. [25] Cellular

heterogeneity is a key indicator of malignancy. Pleomorphism should be evaluated by examining the size, thickness, and colour of nuclear cells. [25]

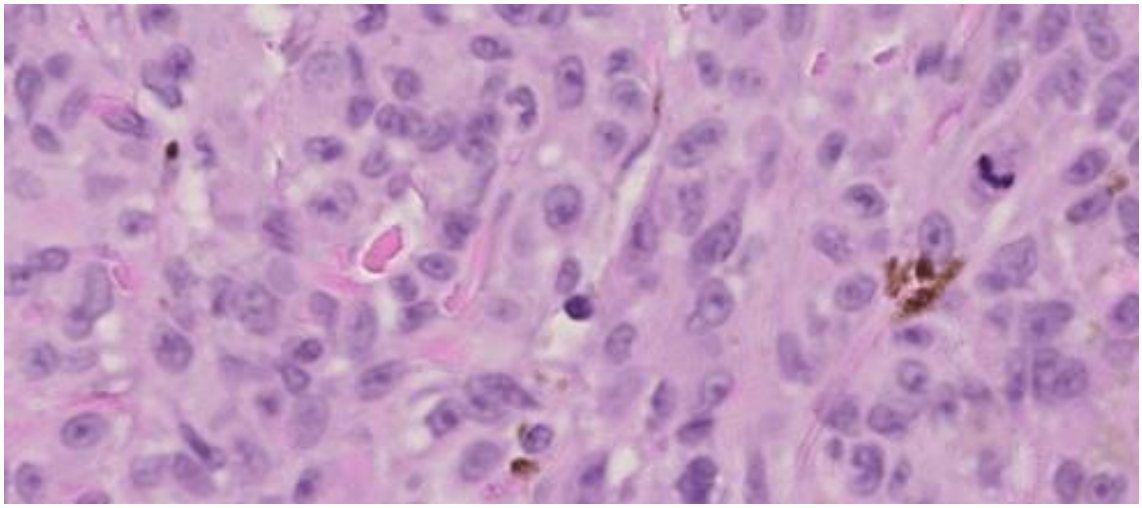

Figure 8- In this cytological milieu, we observe significant nuclear pleomorphism, nuclei with coarse chromatin, and mitoses.

Tumour Breslow Thickness

Melanoma thickness is the strongest predictor of clinical outcome for patients with localized primary cutaneous melanoma.[24,28] In clinical practice, The Breslow thickness measured vertically from the upper edge of the granular layer of the epidermis to the deepest invasive melanoma cells using an ocular micrometre calibrated to the microscope. [35–40]

In case of ulceration and loss of epidermis, melanocyte distribution is assessed from the the ulcer base to the deepest portion of the tumour. Extensions along periappendageal sheaths and areas of regression are excluded from the measurement but should be reported as additional histological findings. This measurement has some limitations, particularly related to human variability and measurement imprecision. [39,40] Despite their expertise, pathologists supported by the ocular of the microscope can examine only a portion of the tumour at a time during the analysis, potentially missing the overall perspective and the global cell distribution. Moreover, the heterogeneity of the slices collected on the same patient could lead to significant thickness variations within the same tumour. Additionally, the Breslow measurement does not account for variations in the thickness of the normal epidermis at different anatomical sites and changes due to tissue fixation.

Special challenges include distinguishing in situ melanoma from superficially invasive melanoma and differentiating invasive melanoma with a nevoid appearance from melanoma associated with a nevus. [41–43]

Human involvement in evaluating Breslow thickness can lead to interobserver variation and estimation errors. [44–47] Possible imprecisions in Breslow thickness measurement has the potential to significantly impact the clinical evaluation of the patient, affecting prognostic estimations and decision management. [48]

The diagnostic criteria for melanoma can be more complex than those mentioned above, with certain types of melanomas displaying completely unique histological features.

Histopathological examination is often complemented by additional diagnostic tools, particularly immunohistochemical (IHC) staining methods and genetic testing, especially when the histological sample is incomplete or the differentiation status of the neoplasm is unclear. [49–51]

Second opinion review of pathology specimens

Second opinion reviews of pathological specimens are a common practice among pathologists, both within the same institution and across different national or international institutions (extradepartmental consultations).[15,25] The recent multidimensional classification by the World Health Organization (WHO) has brought significant changes to the taxonomy of diseases, based on nine distinct pathways and the recognition of new entities characterized by specific morphologies and associated genetic-molecular alterations.[52] Accurate subclassification within these WHO pathways is essential for optimizing treatment and may require additional analyses.[53,54]

Several studies underscore the importance of real-time expert pathological review, especially for the diagnostic clarification of challenging atypical melanocytic lesions. [12,15,55–58] A change in diagnosis for referred melanocytic lesions has been reported in 10-35% of cases, with subsequent changes in management in most of these instances. [12,15,55–58] In a simulated model involving a population of 10,000 individuals undergoing excision of a melanocytic lesion, diagnostic discrepancies were more likely to result in overdiagnosis rather than underdiagnosis of melanoma.[59] In a retrospective study, major

and minor diagnostic disagreements were found in 20.2% and 48.8% of cases, respectively.[60]

Most pathologists seek a second opinion for melanocytic tumours with uncertain malignant potential, moderately dysplastic nevi, early-stage invasive melanomas, or Spitz tumours. [12,15,55–58] The Italian Melanoma Intergroup (IMI) recently established a Second Opinion Consultation Service to provide systematic and timely pathological reviews of newly diagnosed ambiguous melanocytic lesions, further optimizing patient care. [15] Second opinions have been shown to reduce healthcare costs by decreasing both overtreatment and undertreatment. [15] Additionally, second opinions offer valuable learning opportunities for less experienced physicians or those in need of updates in dermatopathology. [55]

However, there are also challenges associated with second opinions. Despite their utility, diagnostic variability among pathologists remains high, even among dermatopathology experts, due to the subjective nature of histopathological interpretation and the lack of objective reference standards for classifying melanocytic lesions. [55,56,61] Moreover, obtaining a second opinion can increase diagnostic costs and delay results, which may be a barrier for some patients or for healthcare systems with limited resources. [55]

In Italy, the National Health Service covers the initial pathological diagnosis for all citizens, regardless of income or age. However, second opinions are not reimbursed and are not currently included in the core benefits package (LEA).[15] Finally, there are no clear and universally accepted guidelines on which cases warrant a second opinion or how to resolve diagnostic disagreements among pathologists. [55]

Immunohistochemical (IHC)

In recent years, IHC has become increasingly valuable in aiding pathologists with melanoma diagnosis, thanks to its widespread availability in most laboratories, as well as its reliability and reproducibility.[62,63] There are two types of biomarkers most commonly used for melanoma diagnosis and prognosis: melanocytic markers and proliferative markers.[64] Melanocytic differentiation markers (S100, SOX10, HMB-45, Melan A/MART-1, MITF, Tyrosinase, KBA 6.2, NKI/beteb, PNL2, MC1R, CD146/Mel-CAM, NKI/C3, and p75NGFR) help determine whether an ambiguous lesion is melanocytic,

while proliferative markers (Ki-67, PHH3) serve as a strong indicator of cell cycle activity, providing insight into the lesion's proliferative potential.[63,64] There is no single perfect biomarker for melanoma, which is why IHC screenings are often conducted using panels of multiple biomarkers. [63,64] Markers useful for the differential diagnosis between CN and CM (p16, p21, p53, PRAME, NKI/beteb, 5-hmC, PTEN, , H3KT, and H3KS); Markers useful for the identification of specific histological subtypes of CN and CM (BRAF V600E, c-Kit/CD117, ROS1, ALK, pan-TRK, BAP-1, β-catenin, PRKAR1A, NF1, and IDH1); Double stains (DS) (HMB-45/Ki67, MART-1/Ki67, D2-40/MITF, D2-40/S-100, D2 40/SOX10, D2-40/MART-1, CD34/SOX10, HMB-45/PRAME, MART-1/PRAME, and MART- 1/PHH3) (Fig.9). [63,64]

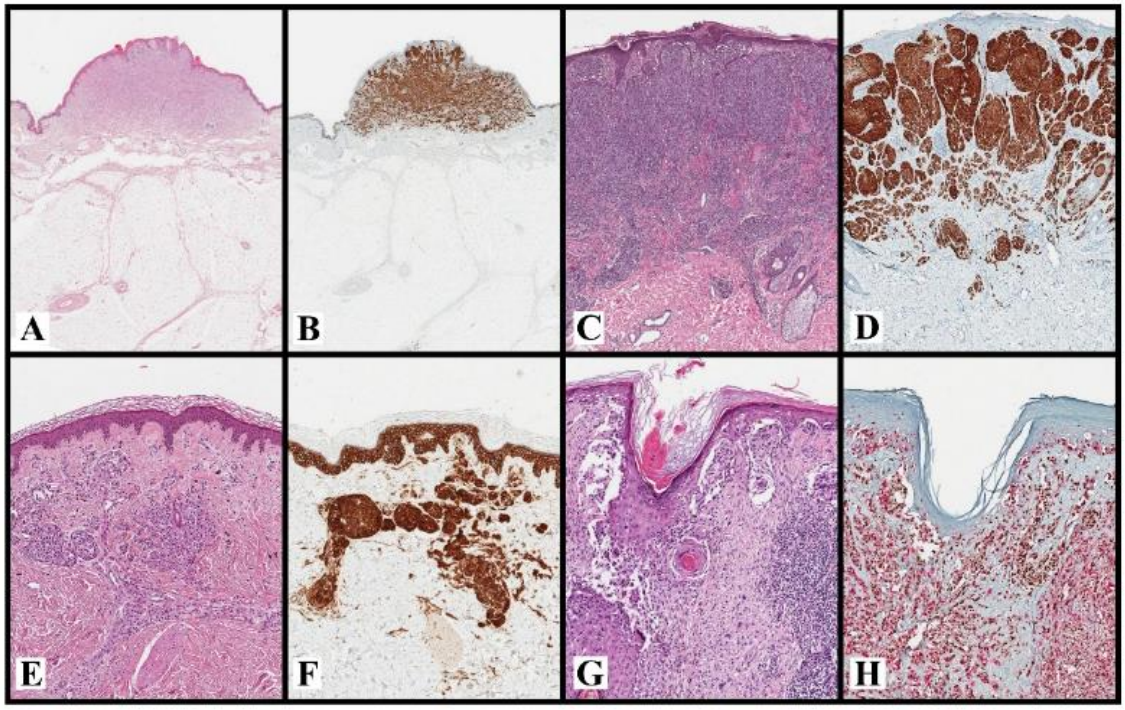

Figure 9: Spitz cN with ALK-translocation (A,B). A case of Spitz cN with a characteristic plexiform morphology ((A): H&E, original magnification ×20), which suggests an ALK translocation and turned out positive for ALK ((B): H&E, original magnification ×20). Spitz cN with NTRK1-translocation (C,D). A case of Spitz cN with filigree-like rete ridges and lobulated nests ((C): H&E, original magnification ×50), which suggests a NTRK1 translocation and turned out positive for NTRK ((D): H&E, original magnification ×50). Deep-penetrating cN with CTNNB1 mutation (E,F). A dermal cN with a wedge-shaped silhouette, large and bland epithelioid melanocytes arranged in small nests, and ill-defined fascicles ((E): H&E, original magnification ×80), which suggests a "deep-penetrating" morphology and turned out positive (cytoplasmatic and nuclear) for β-catenin ((F): H&E, original magnification ×80). Lentigo maligna melanoma (G,H). A lentigo maligna melanoma with single and nested atypical melanocytes that involve the adnexal structures and markedly efface the epidermis ((G): H&E, original magnification ×100). This case turns out positive for HMB-45 (cytoplasmatic) and PRAME (nuclear), with a 4+ score ((H): HMB-45/PRAME, original magnification ×100; HMB-45: red, PRAME: brown). Note that DS HMB-45/PRAME allows us to simultaneously establish the melanocytic nature of the lesion and evaluate the PRAME score. Abbreviations: cN: cutaneous nevus; DS: double staining.

Despite recent advances in genetics, epigenetics, and molecular discoveries that have deepened our understanding of skin cancers, some aspects remain elusive, and H&E histological analysis continues to be the primary, and often the only, tool for diagnostic interpretation worldwide. Furthermore, the ability to conduct complex and costly molecular studies is often limited, particularly in pathology laboratories with constrained financial resources. Therefore, developing new diagnostic techniques for skin tumours is crucial to help pathologists to standardize the diagnoses and to ensure accurate patient treatment planning.

Artificial intelligence in histopatological melanoma diagnosis

With the rise of digital pathology (DP) and the development of advanced computational tools, artificial intelligence applied to histopathology (often referred to as computational pathology) has made significant advancements and attracted growing attention in recent years.[65,66] In DP, the glass slide can be digitized to produce a high-resolution image resembling the one from the microscope, called Whole-Slide Image (WSI).[67] WSIs can be used for primary diagnosis just as successfully as a microscope. Artificial Intelligence (AI) techniques, particularly machine learning (ML) and deep learning (DL), with a focus on convolutional neural networks (CNNs), have proven highly effective for WSI image analysis. CNNs are especially suited to image processing tasks, allowing a fully automate extraction of geometrical and textural features from the image which could be linked to morphological features of the tissues and cells.[65,66]

Early applications of AI in pathology began with interactive programs that integrated histologic data and clinical information. However, it was not until 2003 that AI systems were used to enhance learning through tutoring.[68] In 2005, a hypertext atlas of dermatopathology was created, featuring 3’200 histopathologic images with the potential for continuous updates, highlighting AI's flexibility in education and research. [69]

In skin cancer research, one study first trained a convolutional neural network (CNN) on 129’450 images representing 2’032 skin conditions. The CNN outperformed 21 dermatologists in distinguishing between melanomas and benign nevi, achieving an area under the curve of over 91%. [70] Another study used CNNs to analyse 695 skin lesions,

finding 18-20% disagreement between the CNN and a histopathologist's diagnosis, which closely matched inter-pathologist disagreement rates. [71]

Between 2008 and 2018, a multicentre database was developed with over 2'000 WSI, showing CNNs consistently outperformed human experts in identifying melanoma versus benign nevi. They trained two CNN architectures (namely ResNet-50 and VGG-19) using >9.95 million patches. The CNN is also used to detect cells between nevi and melanoma to make the classifications plausible [72]

Another study showed that CNN ensembles matched the performance of 18 expert dermatopathologists, with sensitivity, specificity and accuracy of 98%, 88%, and 93% respectively, comparable to experts. Despite some diagnostic discrepancies, CNNs showed high reproducibility, particularly when combined into ensembles. [73]

A recent study trained the Fast Random Forest algorithm on 125 histologic images of 63 melanoma patients to reduce variability in diagnosing nevus with high-grade dysplasia and melanoma, achieving 17% discordance. They trained the algorithm to recognize architectural features (such as the arrangement of individual and aggregated melanocytes, and the symmetry or asymmetry of the lesion) and cytologic details (including nuclear atypia, pagetoid spread of melanocytes, and potential necrosis) [66,74]

Overall, AI systems, especially CNNs, have shown great promise in dermatopathology by improving diagnostic accuracy and objectivity, reducing time, and providing a valuable tool for both novice and experienced pathologists. [75]

In addition, AI models can offer quantitative assessments of biomarkers to classify diseases into subtypes and predict patient outcomes.[76] For instance, AI can quantify the density of tumour-infiltrating T cells (TILs), an important prognostic factor, or help identify mitotic figures, which may signal malignancy. [77,78] Traditional methods for detecting mitosis manually are labour-intensive and prone to interobserver variability. AI-based algorithms, particularly CNNs, have been developed to automate this process, learning complex patterns associated with mitosis from large datasets and detecting them with high precision. [78] In a retrospective study, authors developed a DL model using histopathology slides from 108 patients to predict metastasis risk, aiding

dermatopathologists in identifying aggressive tumours and forecasting survival outcomes. [79]

Despite the promise of AI in histopathology, only a small fraction of studies have been approved for clinical use, largely due to the lack of generalizability in their methodologies.[80] One major limitation is the need for large, high-quality training datasets. Developing reliable DL models for WSI analysis requires manually annotated images, a time-consuming and challenging process that demands high precision to ensure accurate segmentation models. [81] Additionally, significant interobserver variability among pathologists complicates the efficient training of AI models. [81]

A key challenge with AI is that its outputs often do not intuitively align with traditional clinical reasoning or human logic. These models frequently operate as "black boxes," producing results without clear explanations of how they reached a specific conclusion.[82] This lack of interpretability hinders trust in AI models and slows their clinical adoption.[80]

Finally, the current limitations of image databases, along with restricted image sharing between institutions, further complicate AI-based diagnosis.[80] While dermatopathologists are trained to consider a wide range of differential diagnoses, most CNNs can only determine if an image is positive or negative for a specific disease.[80]

Mosquera-Zamudio et al.[80] analysed published research on DL methods for automatic image analysis of melanocytic tumour WSIs. The image modalities in the included studies varied significantly, both in terms of the diagnostic information they provide and the technical requirements (e.g., feature types, image sizes, preprocessing). Of the studies reviewed, 13 (41.38%) used only a single data source, typically relying on local datasets, while studies with multiple sources often utilized open-access datasets. Although studies using a single source achieved good results, they face a major limitation when applied to real-world clinical practice. Variations in tissue characteristics between different geographical and ethnic populations, as well as differences in tissue processing (e.g., gross sectioning, fixation, section thickness, staining methods, and scanning), can impact image quality, leading to inconsistencies between pathology labs. Therefore, for DL models to be effectively implemented in clinical practice, they must be trained on datasets from diverse sources. The more variety a model is exposed to, the better it will generalize to accurately predict new, unseen data.[80]

Purpose of the Study

In these paragraphs, we have highlighted both the diagnostic and management challenges faced by histopathologists, including the complexity of diagnosing cutaneous melanoma, the need to streamline workflows, and the development of new diagnostic support methods that can supplement or replace resource-intensive investigations. We have also addressed critical issues associated with AI techniques documented to date. Building on this background, our study introduces a novel AI and statistical learning-based diagnostic approach for cutaneous melanoma. This method could prioritize the review of histopathologic slides in an automated pipeline by distinguishing high-risk melanoma features from low-risk nevus features. Additionally, it could provide a valuable second opinion in challenging cases, such as melanomas arising within nevi or in differentiating DN from CM. This study is organized into three main sections: 1) Automated silhouette definition and its diagnostic value, 2) Nuclei feature extraction and classification modeling, and 3) Evaluation of Breslow thickness.

Automated silhouette definition and its diagnostic power

Material and Methods

This study involved the eDIMESLab and Oncologic Dermatology Unit, IRCCS Azienda Ospedaliero-Universitaria di Bologna. The protocol was approved by the Local Institutional Review Board. Histopathologic slides were collected by the Laboratory of dermatopathology, Dermatology, of the Sant'Orsola-Malpighi Hospital and the digital WSIs were acquired using a NanoZoomer 2.0-RS Hamamatsu scanner with a 40x (0.23 μm/pixel) magnification and auto focusing. Each case was anonymized obscuring the histological image label and an anonymous identification number was assigned in order to guarantee the anonymization of sensitive data. All samples examined derived from deep excisional biopsies or wide excisions. Hematoxylin and Eosin (H&E) stained WSI were reviewed by expert dermatopathologists with >10 years of experience in dermato-oncology. For each patient, multiple WSI slices were collected to guarantee a robust evaluation for the clinical practice. To reduce data redundancy, only non-consecutive slices were considered for the statistical analysis of each patient, when possible.

Histological evaluation included Breslow thickness, mitosis number, presence of ulceration, inflammation, and tumor regression. Clinical data were evaluated for each case, including gender, patients' age at diagnosis, tumor location and clinical diameter of the lesions.

Computer aided diagnosis system pipeline

The entire set of WSIs was analyzed using a multi-resolution image processing pipeline. Starting from the low-resolution level of the WSI pyramid, the entire set of slices was automatically identified using an Otsu thresholding algorithm [83] on the grayscale version of the image, filtering the possible confounders (such as bubbles, dirt, and highlighter marks) on the glass slide. The automatic identification of the epidermis surface by thresholding algorithm can guarantee the rotation of the sample using the epidermis as reference and thus introduce a metric of depth. The identified slice ROIs were used to extract the image information on the highest resolution level (40× magnitude), allowing the focus of the next analyses on the only informative regions of the entire WSI. For each slice, the binary mask of the entire tissue was extracted, defining a representation of the slice contours. According to the slice mask obtained on the low-resolution level of the WSI, a dedicated U-Net segmentation model [84] was applied to identify the contained cells in the highest resolution level. The model was trained on the PanNuke [85] dataset to obtain a detailed description of the cells' contours. The entire image processing pipeline was developed in Python using Openslide [86] and OpenCV packages [87] for the management and analysis of WSI samples.

Silhouette definition

The superposition of the distributions of the detected cells on the original WSI image provides its spatial registration. We further discretized these distributions in altitude levels of intensity: each level groups a range of density scores and we associated a different (incremental) color to each of them for the clinical visualization. The shapes of the resulting density levels act as silhouette descriptor of the neoplastic area. For the visualization of the results and the management of the produced silhouette a dedicated plug-in on the Sedeen Viewer software was developed. The Sedeen Viewer software is supported by the Pathology Image Informatics Platform (PIIP) project by Martel et al.[88]

and thus it provides an easy integration of our pipeline also in other WSI projects. In our application we provided to the clinician also the possibility to turn on/off each level of the density distribution: in this way we guaranteed an incremental accuracy of the density score and we left to the expert the possibility to choose the desired level (Fig. 10).

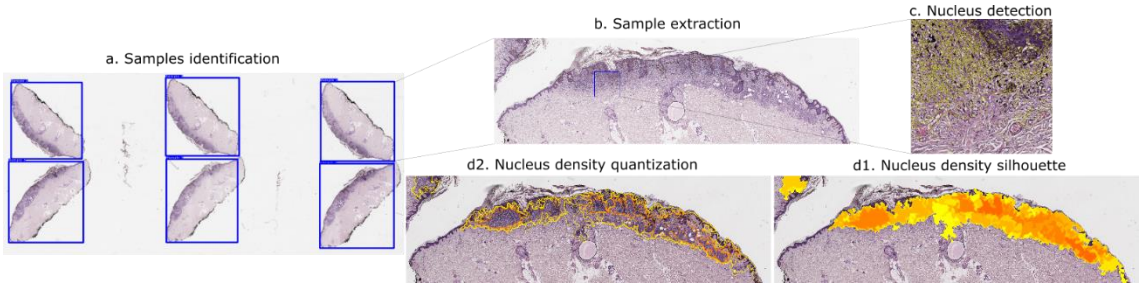

Figure 10 - Heatmap elaboration. a: WSI comprises multiple consecutive sections of a single sample, each of which was analyzed independently; b: Sample extraction with the removal of possible confounding factors, identification of the epidermal surface and the rotation of the section; c: Automated and unsupervised cell identification and classification based on their morphological characteristics; d1-d2: The resulting spatial distribution highlights the density map of the cells in the section and the superimposition of this distribution on the original image allows its spatial registration with the WSI with silhouette delineation.

The slides of 50 CM and 20 CN were included in this analysis. We divided the evaluation of the samples among two experts: 1) the first histopathologist performed the manual annotation of each WSI sample highlighting the melanoma and nevus silhouette; 2) the second expert estimated, with a blinding evaluation, the agreement between the areas identified by his colleague and the result of the automated algorithm. Then, the validated automated silhouettes were submitted to other dermatopathologists. Each silhouette was overlayed on the original WSI, and the opacity of the resulting image was adjusted to partially obscure the underlying histological source. During the blind evaluation, the expert was asked to determine the potential malignancy of the underlying lesion in relation to the silhouette shape. Each section was labelled as “melanoma” or “nevus”, and the results of the blind evaluation were compared to the ground truth diagnosis.

Results

We included 50 patients (28 males and 22 females, mean age 67 and 64 years) with diagnosis of superficial spreading CM and 20 CN (11 males and 9 females, mean age 42.2 years). Clinical and histopathological results are summarized in table 1.

Table 1 - Clinical and histopathological characteristics of 70 patients (50 diagnosed with CM and 20 diagnosed with CN)

Patients	**n**	**%**	**n**	**%**
	melanomas		**nevi**	
Age				
<50	19	38	15	75
50-59	6	12	3	15
60-69	8	16	2	10
>70	17	34	0	0
Gender				
Female	22	44	9	45
Male	28	56	11	55
Location				
Trunk	28	56	15	75
Head and neck	3	6	0	0
Limbs	19	38	5	25
Ulceration				
Absent	49	98		
Present	1	2		
Mitosis (x mm2)				
<1	45	90		
>1	5	10		
Breslow (mm)	*Average*	0,4		
<0,8	44	88		
>= 0,8	6	12		
Regression				
Present	23	46		
Absent	27	54		
Inflammation				
Absent	9	18		
Present: - Brisk - Not-brisk	 11 30	 22 60		
Stage				
pTIS	2	4		
pT1a	42	84		
pT1b	3	6		
pT2a	3	6		

The cells spatial distribution allows a multi-scale overview of the sample at different resolution levels, which are represented by a heatmap overlayed on the WSI. A global overview of the lesion silhouette can be achieved using the low-resolution levels of the WSI. This highlights the melanocytes spatial distribution in both the epidermis and dermis areas, guaranteeing the detection of a possible melanocytes' invasion of the upper epidermis in a pagetoid growth. The qualitative measurement of the melanocytes' structural disorder into the tissue allows a first fast evaluation of the sample. The heatmap is an easy-to-use visualization for assessing the level of clustering of detected cells. In 94% (47/50) of melanomas and 100% (20/20) of nevi analysed, the automated silhouette identified by our method is compatible to those manually contoured by the expert dermatopathologist with a qualitative superiority to the manual scheme in identifying melanocytes. Furthermore, the two pathologists confirm that areas with highest intensities of malignant melanocytes identified by our method correspond to the region of interest for melanoma diagnosis related to the presence of high nuclear density, nuclear atypia, and neo-angiogenesis (Fig.11).

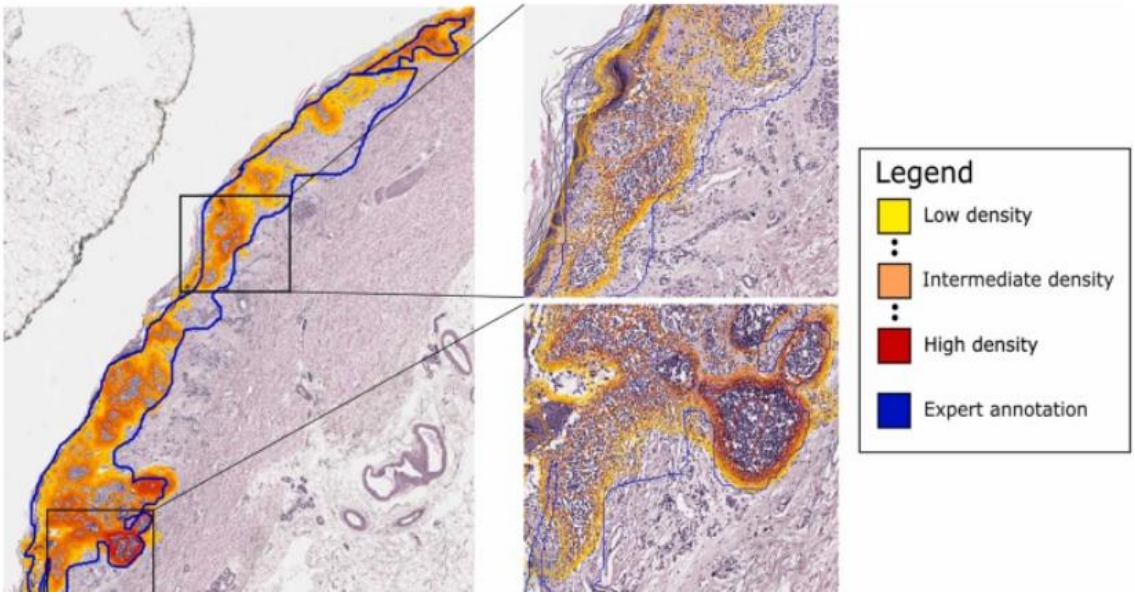

Figure 11 - The silhouette identified by our method is defined by a range of density scores. We used incremental colors (from yellow to red) to represent those levels for the clinical visualization. The method is comparable with the silhouette manually contoured by the expert histopathologist (blue line), and in some cases qualitatively superior in the identification of tumoral areas.

Regarding principal limitations, it was seen that in some cases the automatic identification classified tissue characterized by visible inflammation or skin appendages, such as glands

and hair follicles, as melanoma-like regions. Both biological structures are characterized by a high level of cellular density and, without a following classification of the nuclei, are difficult to discard by the described method.

The validated automated silhouettes were submitted to 2 dermatopathologists. A symmetrical, vertically oriented, wedge-shaped silhouette with a smooth, well-defined edge was associated with a benign lesion; an asymmetrical silhouette with a jagged and poorly defined edge was defined as a malignant lesion. On all the available sections (156), 18% of the silhouettes led the expert to an incorrect diagnosis (melanoma-like silhouette vs. a diagnosis of benign nevus and nevus-like silhouette vs. a diagnosis of melanoma). This non-negligible error rate can be reduced in light of the following consideration: this analysis was performed considering multiple (at least 2 to a maximum of 6) sections for each patient in order to increment the statistical population which added to the robustness of this pipeline; but the identification of CM can be sometimes observed only in fewer sections. Adjusting for this consideration by grouping together the sections belonging to each patient, only 1 patient (4% of error rate) was incorrectly classified by the expert (Fig 12).

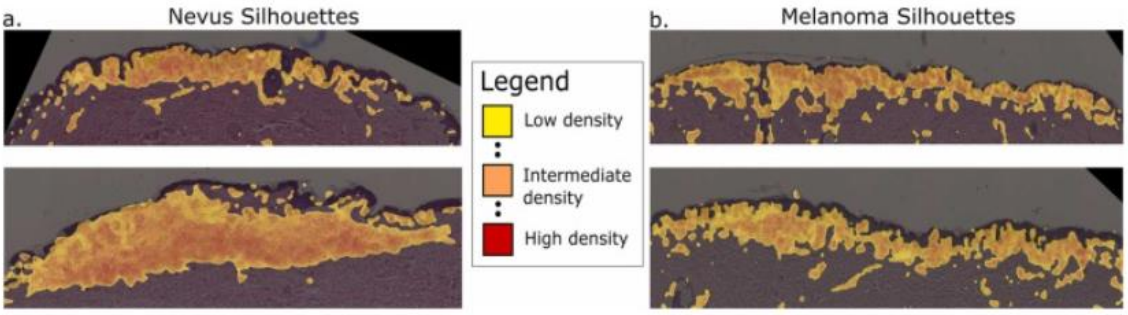

Figure 12 - Examples of benign (left) and malignant (right) lesions in relation to the silhouette shape. The silhouette contour was filled to obtain a dense heatmap of the segmented area and the underlying histological source was partially obscured to focus the attention of the expert on the segmented area. In the case of nevus silhouette, the shapes are symmetrical, vertically oriented, wedge-shaped, and sharply circumscribed with smooth borders and flat base. An asymmetrical silhouette with a jagged and poorly defined edge is defined as a malignant lesion.

Discussion

In the diagnosis of melanocytic skin tumors, the assessment of the overall architectural pattern, the silhouette of the lesion, is fundamental.[20,26,89] The most promising advances in histopathologic diagnosis are supported by new technologies and are based on image

processing techniques.[90–92] Most published studies attempt to exploit deep neural networks in order to assess histomorphological features in H&E slides.[91] However, deep neural network models require extensive training and multiple validation sets. Hekler et al. [91] applied a deep learning algorithm for the first time in histopathological melanoma classification showing a discrepancy between a convolutional neural network and the histopathologist in 19% of the images. These results were comparable to the pathologist interobserver variability described in the literature. [12,20,60] The goal of this model is to overcome the limitations of supervised approaches and, thus, it can be applied without relying on manually labeled samples. In literature, there are several deep learning models proposed to automate the processing of WSI that require manually annotated sets of images in order to obtain reproducible training of the parameters.[93,94] This step is normally difficult and time-consuming to perform at the accuracy level required for a precise segmentation model. Many authors have already proposed automatic pipelines for the segmentation of histological samples, and a major part of them focus the analysis of small patches of each section, usually at lower resolution than the one allowed by the WSI.[90–92,95] This approach guarantees a fast evaluation of the section, but it leads to a rough segmentation of the underlying physiological structures. The proposed method performs the analysis on the entire WSI without the need for a subdivision in patches. Therefore, it is possible to obtain segmentations and silhouettes at high resolution that are therefore easy to use and validate by the experts. The developed pipeline requires an elaboration time compatible with clinical application (an average of about 10 minutes per section). The most time-consuming step (87% of the time) is given by the segmentation and classification of the cells, which requires a high-resolution analysis of the WSI. Additionally, the pipeline can be further optimized using a GPU support. In accordance with Dall'Olio et al.[96], the use of a distributed computing for high memory-consuming data should be discouraged, since the best computational performances are reached by a concurrent parallelization framework. In conclusion, we have shown that the proposed method allows for a quick identification of the most informative regions of interest for diagnosis. The agreement between the human silhouette and the areas identified by the automated algorithm in our study ranged from 94% in melanomas to 100% in nevi and the diagnostic power of these silhouettes was validated by two dermatopathologists. This result shows the importance of the lesion silhouette for the formulation of the

dermatopathological diagnosis and the importance of an accurate detection of the tumor area for the discrimination between benign and malignant skin lesions.

Nuclei features extraction and classification model

Material and Methods

This study involved the the Department of Statistical Sciences (UNIBO), the Department of Physics and Astronomy (UNIBO) and Oncologic Dermatology Unit, IRCCS Azienda Ospedaliero-Universitaria di Bologna. The slides of 40 CM, 20 CN and 40 DN with a total of 146 samples, were selected for a statistical learning analysis based on nuclear morphological features and their spatial distribution. Firstly, the acquisition of the digital WSIs and the multi-resolution image processing pipeline to segment cells described in the previous chapter was applied to the set of WSIs included in this study to segment cells. Then, the data preparation process followed further steps that are described in the next paragraphs.

Nuclei Features Extraction

The cells' masks collected on the entire dataset involved the analysis of more than 6 million nuclei that were analysed to characterize their morphology and textural aspects. For each cell, the corresponding contour of the binary mask was extracted, and the component was characterized using 16 morphological features (e.g. area, perimeter, circularity, elongation, etc.) and 35 textural features (e.g. RGB, HSV, and Lab averages and variances, Haralick features [97] etc.). Associated to each cell, its spatial position on the slice was estimated considering the barycentre of its contour shape. The spatial coordinates of each cell were rescaled according to the PCA coordinates systems, providing information about their spatial distribution in relation to the epidermis layer. 146 samples from the cell segmentation process were further summarized to build a set of variables that can describe the peculiarities of the different slides. This statistical processing of the samples, along with the subsequent analyses, has been carried out in R. The first step of the process involved the identification of the lesion in each slice. To this aim, the larger clusters of cells obtained by the HDBSCAN[98] algorithm were isolated. Indeed, such a method is a density-based clustering algorithm that allows us to identify

groups of units (cells in our case) being connected according to measures related to the concept of density. (Fig.13)

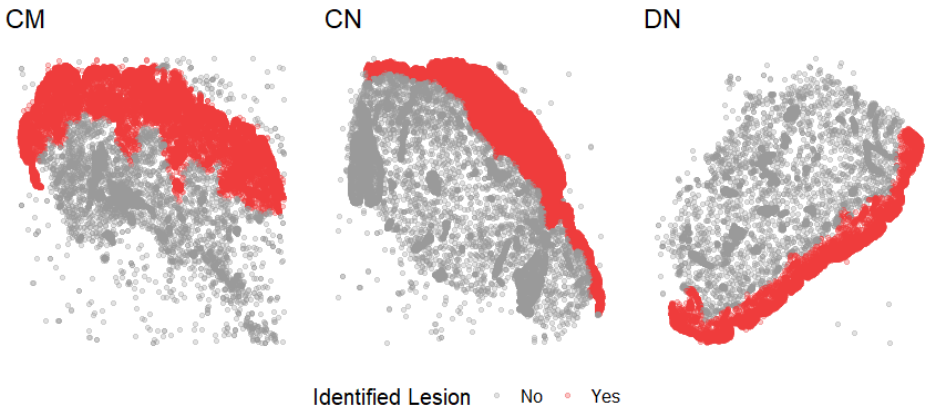

Figure 13 - Example of lesion identified by the HDBSCAN algorithm (in red) for each kind diagnosis.

Subsequently, focusing on the cells constituting the lesion, the behaviours of cell area (A), aspect ratio (AR), extent (E), and sphericity (S) were investigated, noting that their spatial distributions vary over the sample area. (Fig.14)

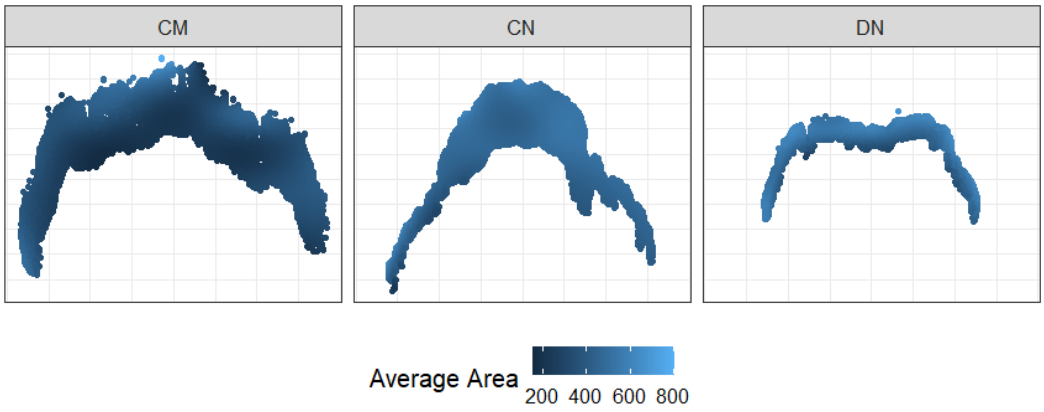

Figure 14 - Example of the distribution of average cell sphericity and average cell area across the four samples. This image illustrates how the spatial distribution of these features can vary within the sample area, highlighting that summarizing these variations is crucial for providing valuable information to differentiate between diagnoses.

Since it is known that the studied lesions can manifest different cell characteristics with respect to their depth (Fig.15), these patterns were summarized by splitting the cells into different strata, namely four groups (labelled with *S1*, *S2, S3*, and *S4*) determined by the quartiles of the distances (Fig.16). As the fourth group of cells can display irregular

behaviour, it was excluded from the analysis. Then, in each stratum, the mean and the standard deviation (*sd*) of the cell attributes were computed (e.g. *E_S2_mean* will indicate the mean cell extent in the second stratum). To evaluate the heterogeneity of these features across the strata, the between-strata standard deviation was also computed (named, e.g., *E_sd_bet*), being defined as the standard deviation of the means obtained in the different strata of cells.

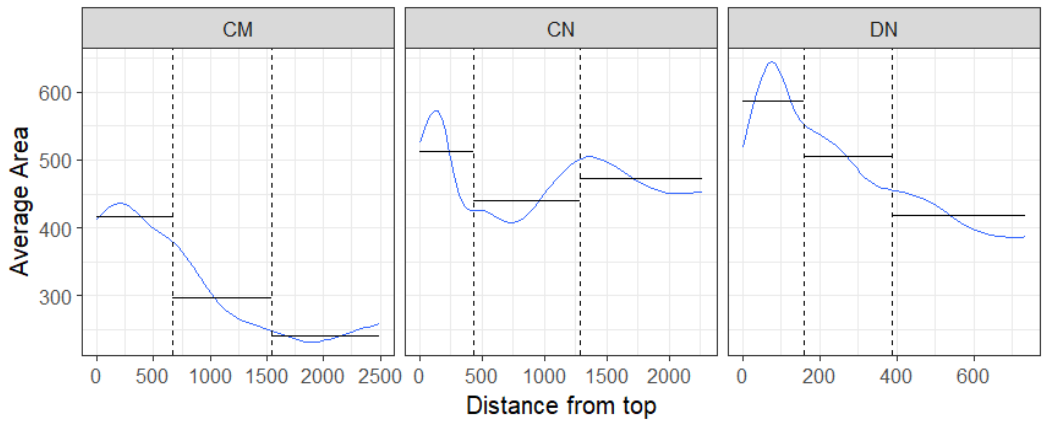

Figure 15 - the blue lines emphasize the non-linear trends in the relationships between the features considered (sphericity and area) and the distance of the cells from the top. The vertical dashed lines identify the first 3 strata, included in the analysis (labelled with S1, S2 and S3); whereas the horizontal lines represent the average values of the cell features belonging to the different strata.

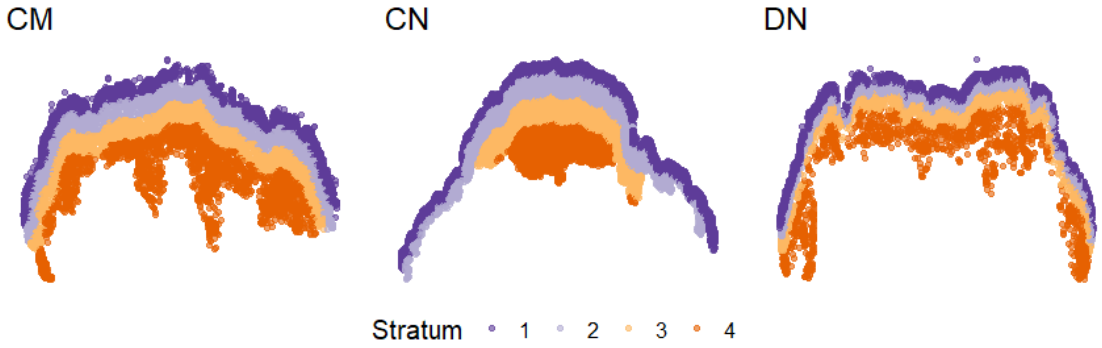

Figure 16- To get information to use in statistical learning models, the lesion silhouette are summarized by splitting the cells into different strata, namely four groups determined by the quartiles of the distances

A further useful aspect to include in the analysis regards the spatial correlation of the features measured on the segmented cells, i.e. evaluating if similar cells tend to be clustered or not. To this aim, basic descriptive geostatistical tools [99] can be useful and we fit the Spherical and the Exponential variogram models on the empirical variogram using

the R package *gstat* [100]. The best variogram model is selected in terms of Akaike Information Criterion. The area feature showed a marked spatial correlation that we summarized in three typical variogram parameters: *A_Range*, *A_Nugget*, and *A_Sill*. Another set of computed variables had the goal of describing the relationship among cells, relying on the distribution of the nearest neighbor distances (NND), evaluated through the *spatstat* R package [101]. The NND distributions were summarized in the whole lesion and in the *central* part (S2+S3) through the median (*med*), standard deviation, and first and third quantiles (*q1* and *q3*). Lastly, we included in the analysed dataset the number of cells, the strata widths, and the density of cells in S1. In this way, 44 variables that describe the lesions included in the sample are available.

Classification Model

We studied several supervised classification techniques, concluding that the most interesting results were obtained considering the family of methods comprising Linear Discriminant Analysis (LDA) and Quadratic Discriminant Analysis (QDA) [102]. In more detail, we applied LDA to the entire set of variables, obtaining an optimal subset through a stepwise forward selection algorithm based on Wilks' Lambda criterion. As a benchmark, we also consider Regularized Discriminant Analysis (RDA) [103], which automatically handles potential multicollinearity issues and combines the group covariance matrices used in LDA with the more general definition of QDA. This is reached at the cost of losing the interpretability of the discriminant directions that characterize LDA. All functions needed to implement these methods are available in R within the packages MASS [104] and klaR [105].

To evaluate the effectiveness of model classifications a Monte Carlo Cross-Validation (MCCV) study is performed by randomly splitting 200 times the whole dataset into a training set (85%) and a test set (15%). Then, the trained models were used to classify the samples in the test set, obtaining false negatives (FN), false positives (FP), true negatives (TN), and true positives (TP). At each iteration, we computed:

accuracy = TN+TPFN+FP+TN+TP,

sensitivity = TPTP+FN,

precision = TPTP+FP,

F1=2TP2TP+FP+FN,

MCC = TPTN-FPFN(TP+FP)(TP+FN)(TN+FP)(TN+FN),

and we report their average as output.

Results

We included 40 patients with diagnosis of superficial spreading CM (23 males and 17 females), 20 CN (11 males and 9 females), 40 DN (19 males and 21 females). Clinical and histopathological results are summarized in table 2.

Table 2 - Clinical and histopathological characteristics of 100 patients (40 diagnosed with CM and 20 diagnosed with CN and 40 diagnosed with DN).

Patients	**n**	**%**	**n**	**%**	**n**	**%**
	melanomas		**Congenital nevi**		**Dysplastic nevi**	
Age						
<50	11	27.5	13	65	21	52.5
50-59	8	20	4	20	5	12.5
60-69	9	22.5	3	15	8	20
>70	12	30	0	0	6	15
Gender						
Female	17	42.5	9	45	21	52.5
Male	23	57.5	11	55	19	47.5
Location						
Trunk	25	62.5	9	45	26	65
Head and neck	1	2.5	0	0	0	0
Limbs	14	35	11	55	14	35
No Ulceration						
Mitosis (x mm2)						
<1	39	97.5				
>1	1	2.5				
Breslow (mm) ≤ 0,8 with average of 0.5						
Regression						
Present	29	72.5				
Absent	11	27.5				
Inflammation						
Absent	8	20				
Present:						

Patients	n	%	n	%	n	%
	melanomas		Congenital nevi		Dysplastic nevi	
- Brisk	15	37.5				
- Not-brisk	17	42.5				

We applied the proposed image processing pipeline on a dataset composed by 146 histological slices, analysing the spatial statistics variables of nuclei geometrical features and their distributions. A preliminary variable selection step was performed, obtaining 18 relevant variables, listed in Table 3.

Table 3 – Means of relevant variables in the different groups. The superscript letters denote groups that are significantly different, based on post-hoc comparisons from a Kruskal-Wallis test.

	CM	DN	CN
A_S1_mean	-0.107[a]	0.246[b]	-0.419[b]
A_S2_sd	0.081[a]	0.220[a]	-0.684[b]
A_S3_sd	-0.331[a]	0.529[b]	-0.723[c]
A_S3_mean	-0.275[a]	-0.080[b]	0.678[b]
A_sd_bet	-0.031[a]	0.450[b]	-1.055[c]
AR_S2_sd	0.260[a]	-0.158[b]	-0.065[b]
S_S2_sd	0.242[a]	-0.155[ab]	-0.041[b]
S_S2_mean	-0.321[a]	0.139[a]	0.218[b]
S_S3_mean	0.229[a]	-0.355[a]	0.474[b]
E_S3_sd	-0.334[a]	0.445[a]	-0.512[b]
E_sd_bet	-0.366[a]	0.566[b]	-0.754[c]
A_Range	0.498[a]	-0.338[b]	-0.040[c]
A_Nugget	-0.037[a]	0.338[a]	-0.769[b]
Width_S1	0.263[a]	-0.464[a]	0.684[b]
Width_S2	0.158[a]	-0.372[a]	0.640[b]
NND_central_med	0.100[a]	0.087[ab]	-0.390[b]
NND_central_q1	-0.100[a]	0.124[a]	-0.130[a]
NND_q3	0.275[a]	0.095[b]	-0.716[c]

To assess the effectiveness of the classification methods (CM vs. not CM) we conducted the MCCV study, whose results are reported in Table 4. By labelling melanoma samples

as 'positive', the sensitivity index (0.844) provides insight into the effectiveness of the classification method in detecting actual cases. This high sensitivity is coupled with a precision of 0.865, indicating that the classification method does not excessively overestimate the number of predicted melanomas. As a summary measure related to the cases detection, the obtained F1 score is good (0.842). Additionally, the overall classification accuracy is high (0.904), further supported by a robust MCC of 0.783. We also highlight that LDA performed on an optimal subset of variables outperforms RDA, according to the considered metrics.

Table 4 – Values of the indices used to evaluate the classification ability through the MCCV study.

	Accuracy	**Sensitivity**	**Precision**	**MCC**	**F1 Score**
LDA	0.904	0.844	0.865	0.783	0.842
RDA	0.877	0.850	0.796	0.730	0.808

One appealing feature of the LDA classification method is its interpretability, leveraging the dimensionality reduction properties of the technique to shed light on the classification process. Figure 17 shows the scores of the entire set of samples projected onto the two-dimensional space defined by LDA, which represents linear combinations of the original variables that maximize the ratio of between-group to within-group variance. The 95% confidence ellipses indicate good group separation, with the right-hand-side plot highlighting CMs near the CN group, which may reflect the presence of CM cases overlapping with CN. The first linear discriminant (LD) axis accounts for 59.3% of the between-group/within-group variance ratio, mainly separating DN (on the right) from CN and CM (on the left), with CN showing higher scores along the second LD axis. Figure 2 also shows the discriminant coefficients (arrows), indicating the direction of the most relevant variable contributions on the LD axes. This output should be interpreted alongside Table 3, which lists the mean values of variables for each sample group. The superscript letters denote groups that are significantly different, based on post-hoc comparisons from a Kruskal-Wallis test ($a=0.05$), with the p-values adjusted for multiple comparisons using the multivariate t method.

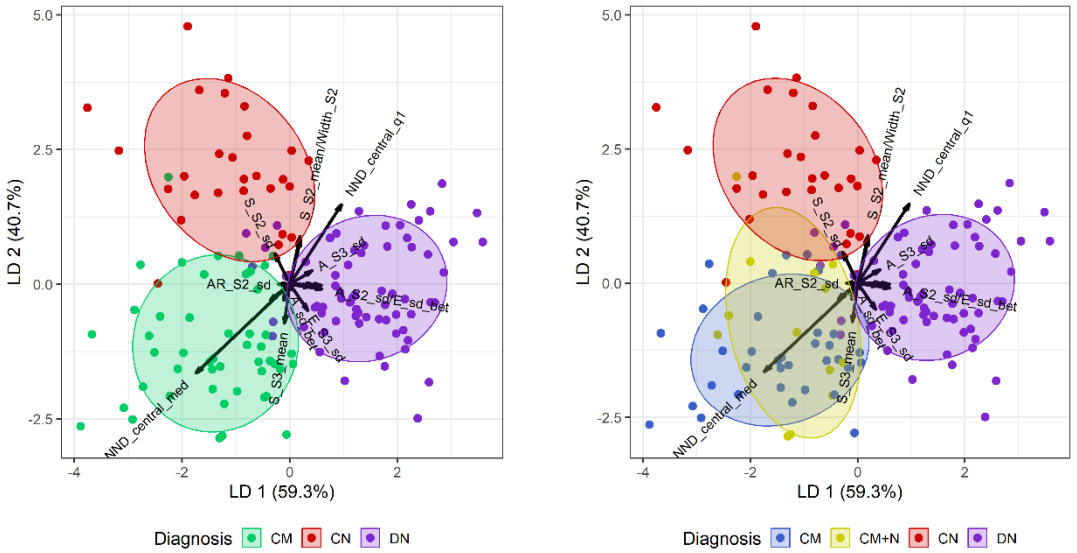

Figure 17 - Scores of the samples projected in the 2-dimensional space produced by the LDA, reporting the 95% confidence ellipses to highlight the groups. Arrows indicate the direction of the most relevant variables for the samples discrimination (discriminant coefficients).

Discussion

The primary challenge in applying artificial intelligence to dermatopathology is the lack of generalizability in existing methodologies.[80-82] Most convolutional neural networks (CNNs) and other machine learning techniques are trained to classify images as positive or negative for specific diseases using "black box" models. [80-82] These models often produce outputs that are not intuitively interpretable using traditional clinical parameters or human logic. [80-82] Furthermore, current image databases are inadequate, and limited sharing of images between sources complicates AI-based diagnoses even further. [66,73,81,91]

In this work, an important outcome of the implemented methodology is the ability to interpret the classification rule from a histopathological perspective, as LDA is not considered a black-box approach. Two histopathologists validated the diagnostic significance of sample characteristics related to nuclear distribution and features. They identified key aspects of nuclear and cellular morphology as crucial for accurate histological diagnosis. For instance, in clinical practice, one method to assess cytological symmetry is to draw a series of parallel transverse lines across the lesion.[25] In a melanoma, the cytological features within each section are distinctly varied. [25] In contrast, a benign nevus displays a consistent cytological pattern throughout the entire layer.[25] Greater variability in nuclear area and sphericity in the second skin layer (A_S2_sd and

S_S2_sd) may be attributed to increased pleomorphism associated with atypical melanocytes. This distinction aids in differentiating between CN, characterized by more uniform nuclei, and CM or CN, both of which can exhibit nuclear and cellular atypia. Moreover, the median nearest-neighbor distance (NND_central_med) is greater in CM compared to other groups, likely due to the higher prevalence of atypical melanocytes, where the nucleus tends to shift off-center, increasing its distance from surrounding nuclei. Lastly, another finding consistent with expected histological behavior is the clustering of nuclei with similar sizes in CM. This is reflected by higher values of the variogram range (A_range), indicating a slower decay of spatial correlation. Such clustering can be explained by the monoclonal proliferation of similar cells in localized areas or clusters, particularly as tumor cells separate from skip areas. [25] These results underline the importance of cellular and nuclear composition in distinguishing between benign and malignant skin lesions in dermatopathology.

We reported the effectiveness of the classification method in detecting melanoma, which demonstrated a sensitivity index of 0.844 and a precision of 0.865. These results indicate that the classification method does not significantly overestimate the number of predicted melanomas. The classification results are obtained under a Bayes classifier approach, to maximize the overall accuracy. However, from a clinical perspective, this may not be ideal, as the two types of classification errors carry different levels of severity. For instance, failing to diagnose a case of CM is far more critical than incorrectly labeling a benign lesion as CM. To address this imbalance, the threshold for assigning the CM label can be lowered, increasing sensitivity. However, this comes at the cost of reduced precision and, subsequently, lower overall accuracy.

We aim to further improve and extend this method for application to other histological entities.

Evaluating Breslow thickness

Material and Methods

The study was performed at the Oncologic Dermatology Unit, IRCCS Azienda Ospedaliero-Universitaria di Bologna with the collaboration of the Department of Physics and Astronomy (UNIBO). 40 WSI slides of CM, reported in table 2, were reviewed.

We asked an expert histopathologist to re-label the entire set of slices according to the Breslow thickness, using their digitised versions in a blind evaluation. This second evaluation was performed using the Sedeen Viewer software supported by the Pathology Image Informatics Platform (PIIP)[106] asking the histopathologist to draw a segment between the deepest melanocyte manually identified in the slice and the granular layer surface. This measurement was conducted without limits of time, allowing the use of the entire set of magnitudes (between 0.1x and 40x) according to the histopathologist's needs. For each identified segment, the coordinates of the starting and ending points were saved at pixel level and converted into micrometre according to the scale factor of the WSI sample. Starting from the same melanocyte identified by this procedure, we asked other 5 histopathologists to evaluate the Breslow thickness on the entire set of WSI samples. Keeping track of the starting point of the measurement, the integration of other histopathologists guaranteed the monitoring of both the Breslow thickness and orientation of the 'ruler' during the evaluation. A dedicated computer vision software was developed for the semi-automated analysis of the digitised WSI samples.

Starting from a manually identified region of interest related to the top area of the slice, i.e. starting from the epidermis surface of each slice, and based on the annotation provided by Operator 1, the application of a series of artificial intelligence models allowed the automated identification of the granular layer surface and the entire set of cells in the tissue. The centroid of each identified cell was used as reference for its position in the tissue, evaluating its Euclidean distance from the granular layer shape. The evaluation of the geodesic distance from the tissue surface provided information about the spatial distribution of the cells and guaranteed the mathematically correct evaluation of the Breslow thickness in each point of the slice (Geodesic in the next), for each identified cell. The possibility to obtain a fully automated Breslow estimation starting from these

preliminary results relies on the possibility to have the classification of all the identified cells. The statistical significance between the measurements of the operators was assessed using paired T-tests between Breslow values. The distributions of slopes produced during the measurements were analysed for all the operators (7 in total), and the spread was put in correlation with the spread in Breslow thickness estimation, to investigate how much of Breslow variance originated from choosing the direction.

Results

In the first analysis we evaluated the accordance between the Breslow thickness measurements performed by Operator 1 and Operator 2. We would like to stress that since Operator 1 performed their evaluation without the help of digitised data, the only term of comparison between the two operators was the Breslow score, without a direct comparison of the exact location in which the measurement was performed. The paired T-test between the two sets of measurements over the 40 available samples produced a p-value of 0.47, showing no significant disagreement between the two operators. Nevertheless, it is important to notice that, despite the not significance of the obtained p-value, the difference between the two operators was estimated as 23.2 ± 200.2 μm, confirming the presence of a bias between them that cannot be captured in terms of statistical test by the high heterogeneity of the two distributions of values.

Using as a starting point the melanocyte identified by Operator 1, the mathematical minimum distance between it and the granular layer of the slice, i.e. the geodesic distance, was evaluated using the information extracted by the proposed semi-supervised software. (Fig. 18)

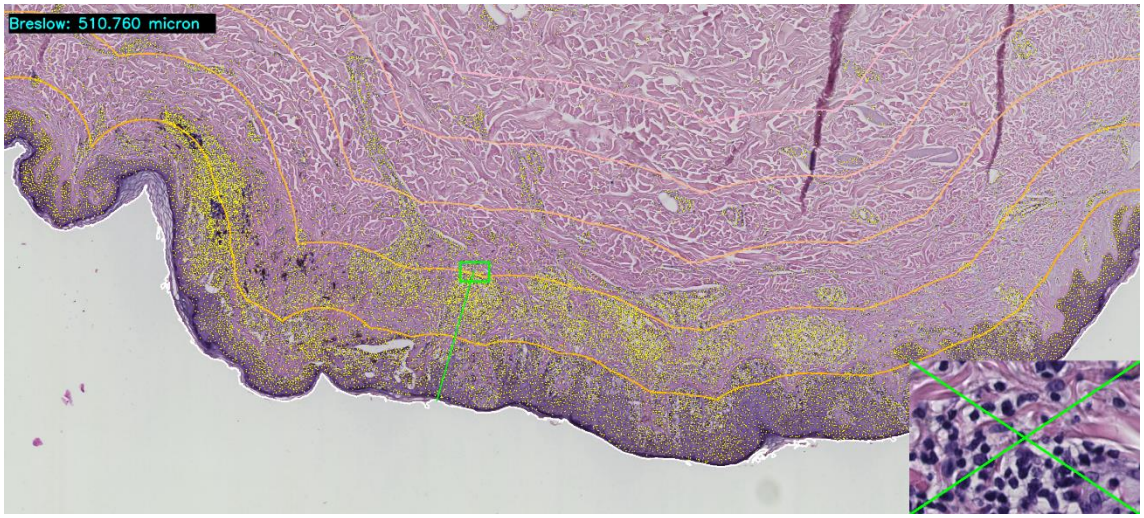

Figure 18 - User interface of the semi-automated software developed for the Breslow evaluation. Artificial intelligence models are employed to identify all cells in the tissue and delineate the granular layer surface. The coordinates of each identified cell are used to automatically compute the geodesic distance from the granular layer surface, which is then displayed in the upper-left corner of the viewer. In the bottom-right corner, a high-resolution region of interest (ROI) at 40x magnification is shown to ensure accurate identification of cell populations. Depth isolines from the granular layer are displayed in varying intensities of orange. Users can manually select the desired location for measurement, obtaining the Breslow thickness at that point with higher precision than standard clinical practice.

The linear regression between the two sets of measurements obtained an R^2 of 0.99 ($y = 0.97x$, p-value ≤ 0.001), confirming the robust agreement between them. However, the evaluation of this kind of regression is significantly biassed using the same starting point: confirming this, the paired T-test between the two distributions of measurements leaded to a (partially) significant p-value of 0.02, with an average difference of 2.5 ± 45 µm. This result pointed out the difficulty of a human evaluator in the estimation of a geodetic distance between a point and a curved line like the complex shape of the granular layer achieved by the fixation process.

The inclusion of the other 5 operators allowed us to increase the statistics of the measurements and the robustness of our hypothesis. Despite the not significant difference between the measurements of all the 7 operators among them, 5/7 of them showed a statistically significant difference if compared with the mathematical geodesic distance. The results obtained by the paired T-test evaluations over the 7 available operators in the Breslow evaluation are reported in Figure 19

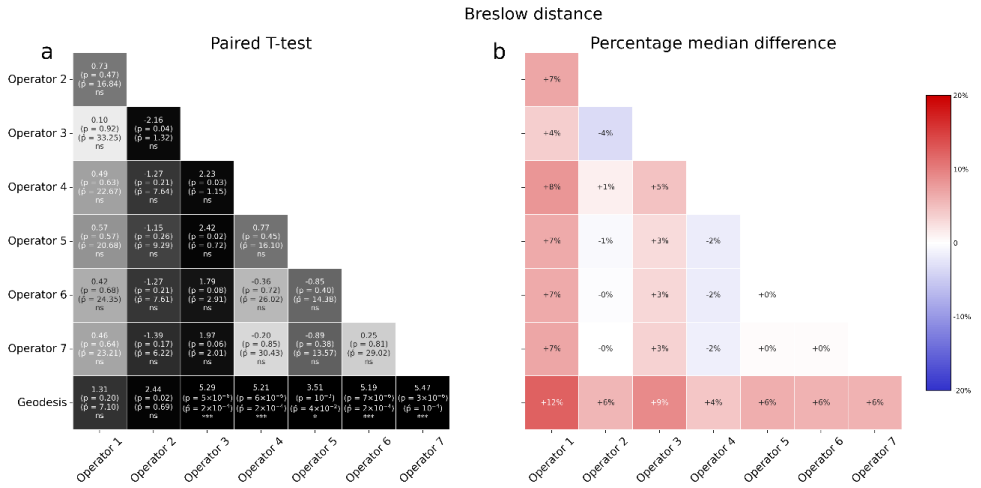

Figure 19 - Statistical results obtained by the comparison of the Breslow measurements collected over 7 histopathologists and the geodesic distance. a. Paired T-test between the 8 sets of Breslow measurements: for each test we reported the T statistic value, the corresponding p-value, and the adjusted p-value corrected by multiple tests (Benjamini–Hochberg); the statistical significance of the test was evaluated on the adjusted p-value, using one or more stars (*) for the nomenclature of the levels (0.05, 0.01, 0.001). b. Percentage of difference between the median values of the 8 sets of Breslow measurements: for each combination of variables we evaluated the difference between the two medians, normalising the results by the first value; we coloured the percentage difference in reds for positive differences and in blues for negative values.

A more readable indication about the differences between the 7 operators could be obtained considering the percentage difference between the medians of the Breslow distributions (Fig. 20), in which we can easily notice how, despite the intrinsic variability between the human operators, there is a common overestimation trend when we compare them with the geodesic distance.

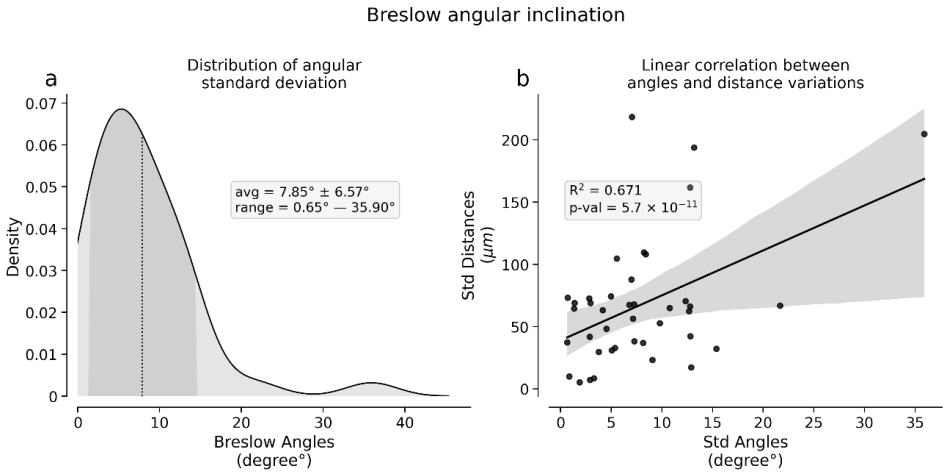

Figure 202 - Statistical results obtained by the comparison of the angular inclinations produced by 6 histopathologists during Breslow measurement, starting from the same melanocyte. a. Distribution of the standard deviations of the angle distributions over 40 histological samples performed by 6 histopathologists; the average angle values ± standard deviation and the range of the distribution domain are reported in the box. b. Linear correlation between the variability of the angle values and variability of the resulting Breslow distances; the R^2 score and corresponding p-value of the linear regression are reported in the box.

To further describe the measurement errors and their cause during human evaluation, we analysed the variability of the angles of inclinations produced by the 6 operators for whom we had the information about starting and ending points, i.e. Operators 2–7. Considering the distributions of angles produced by the 6 operators, we analysed their standard deviations, using these metrics as indicators. The results obtained by our analyses are shown in Figure 20. The variability (intended as standard deviation) of the angles produced by the 6 operators ranged from a minimum of 0.65° to a maximum of 35.90° (ref. Figure 20a), showing an extreme variability during the measurements. Confirming this, we obtained a significant linear regression ($y = 0.32x$, R^2 of 0.67, Pearson correlation of 0.82, p-value ≤ 0.001) between the variability of the angles and the variability of the Breslow thickness estimations (ref. Figure 20b). This result confirms the quite intuitive link between the variability of a distance measure and the heterogeneity of the possible ways in which it was acquired. However, the implication of this kind of correlations in the current context could lead to significant clinical ambiguities, showing the intrinsic human issues in considering this type of measurements.

By evaluating the overall spatial distribution of cells, we observed a significant correlation between the distances annotated by Operator 2 and the 80th percentile of the cell distribution ($y = 0.88x$, R^2 of 0.92, Pearson correlation of 0.96, p-value ≤ 0.001). Examples of the obtained distributions are shown in Figure 21.

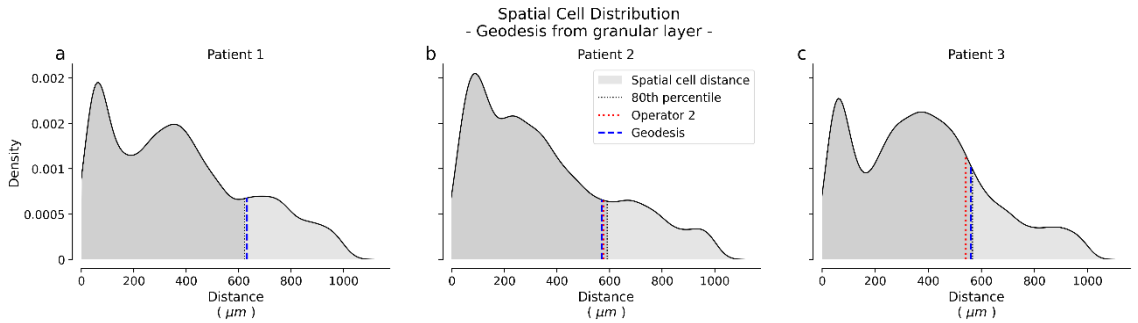

Figure 21 - Distribution of the distances evaluated from each cell and the corresponding granular layer in 3 different slices. a–c. For each cell automatically identified in the tissue by the artificial intelligence model, we reported the distribution of euclidean distances from their position and the identified granular layer; the set of geodesic distances could help the histopathologist in the correct measurement of the Breslow thickness, after the identification of the deepest melanocyte; the manually annotated Breslow distance could be approximated with the 80th percentile of the distance distribution, or, alternatively, with a fixed density value of the cell population, i.e. the distance in which the sparsity of the cell in the tissue surpasses a predetermined threshold.

Discussion

In 1970, Alexander Breslow proposed that measuring melanoma thickness from the skin surface to the deepest point of invasion was an indicator of tumour burden and a prognostic feature for recurrence or metastasis.[24] In 2009, the AJCC confirmed the prognostic significance of Breslow's thickness [107]: the 10-year survival is 92% among the patients with T1 melanomas (0.1 – 1.0 mm) and is 50% in patients with T4 melanomas (≥ 4.1 mm). Over time, many studies have confirmed that tumour thickness is the single most important survival predictor for melanoma. [108,109] However, the correlation between thickness and prognosis is not absolute. [110] A small number of patients with the so-called "thin" melanoma (usually defined as a lesion with depth less than 0.8 mm in the last AJCC version) develop metastases and some with thick melanoma do not. [111–113] Beyond the limits determined by the pathologist's experience and its ability with the microscope, we need to pay attention to a second series of potential issues linked to the measurement process itself. In any kind of distance measurement, like the Breslow one, we always introduce two main sources of errors: i) the definition of the starting and ending points of our measure and ii) the orientation of the instrument used. These two sources of uncertainty are intrinsic in any kind of measurement, posing a limit on the reliability of our estimations. Furthermore, if the first error could be classified as 'random error' and therefore minimised increasing the statistics of our acquisition, the second one could represent a 'systematic error' type due to a personal bias of the pathologist. While approximating a melanocyte as a single point may not result in significant information loss, this is not the case for the granular layer surface. The epidermal layer is typically a curved line with several invaginations, and the section fixation process often causes shrinkage and additional curvature, further affecting the accuracy of measurements and the correct identification of the orientation of the micrometre. Our results emphasise the critical importance of Breslow measurements, which focus on the distance between a single cell and the shape of the granular layer shape. Significant variations in distances measured by different operators can be attributed to the subjective nature of the measurement, which depends on identifying a single point in the tissue slice (the minimum distance of a melanocyte from the skin). Statistically, any measurement based on a single outlier is prone to high variability, making it preferable to use more robust statistical indicators. An objective comparison between the Breslow definition and the spatial distribution of cells can be made by evaluating the distances between all cells and

the granular layer. Beyond these practical difficulties, it is interesting to note that in his initial work, Breslow identified the histological characteristic with the most robust and reliable prognostic potential for melanoma, despite the lack of evidence supporting the view that Breslow's index is related to tumour burden. [110,114] Instead, tumour thickness, serving as a quantitative marker for the biological behaviour that drives melanoma cells progression and invasion. Several studies have attempted to identify miRNA dysregulation and gene expression associated with Breslow's thickness. [115–117] The proteins whose expression correlates with tumour thickness are often involved in cell adhesion, cell survival and invasion. [115,116,118] In particular, E-cadherin, a keratinocyte-melanoma adhesion molecule, experiences a loss of expression early in melanoma progression, which is associated with increased tumour motility and invasiveness. [119,120] Moreover, this mechanism results in altered signalling, leading to decreased apoptosis and evasion of senescence. [121–123]

In this perspective, Breslow thickness does not represent tumour mass but rather the tendency of melanoma cells towards motility, invasion, and progression. Therefore, it is important to consider cell density and the spatial distribution of cells in the slice to better contextualise the measurement of tumour thickness. The importance of cell distribution is underscored by the reasonable assumption that two melanomas with the same Breslow thickness, but different cell densities at the measurement point, may have different invasiveness and prognostic tendencies. The one with fewer invasive cells will likely have a better prognosis. The term 'Breslow density' was introduced in 2017 [40] to describe an estimate of the melanoma cell area at the position where Breslow thickness is measured. This was done to demonstrate proof of concept that Breslow density could be a viable, simple, and reproducible morphological prognostic biomarker and to determine whether detailed future evaluation is warranted. The combination of Breslow density and thickness shows a marginal improvement in predicting 5-years survival. [40]

These studies highlight the importance of correlating Breslow thickness with the distribution and density of all cells in the preparation. Our analysis found a significant correlation between the distance annotated by Operator 2 and the 80th percentile of the cell distribution on the slide. By rethinking the measurement in these terms, Breslow thickness could be associated with the distance from the granular layer for about 80% of

the entire cell population, providing a more robust statistical metric that does not rely on identifying a specific cell. This result underscores the importance of incorporating artificial intelligence in digital pathology as a potential solution to refine standard histopathological measurements, ultimately redefining them with more reliable statistical indicators that minimise human subjectivity.

Conclusion

Artificial intelligence in dermatopathology cannot replace the human element in medical care; however, it plays a crucial role in streamlining workflows and improving diagnostic accuracy. Automating clinical procedures provides invaluable support for both laboratory and clinical practice, leading to faster and more reliable sample evaluations. Our study can expedite WSI screening by prioritizing histopathology slides that exhibit high-risk melanoma features over those with low-risk nevus characteristics.

Furthermore, it can improve diagnostic accuracy in differentiating between benign and malignant skin lesions, assisting in tumour classification and reducing interobserver variability among pathologists, even in challenging cases such as dysplastic nevi and melanomas associated with nevi.

Overall, this model has significant potential to advance clinical workflows and diagnostic practices in dermatopathology, offering an "automated second opinion" that can inform the final diagnostic decision in a timely and consistent manner.

References

1. Sung, H. *et al.* Global Cancer Statistics 2020: GLOBOCAN Estimates of Incidence and Mortality Worldwide for 36 Cancers in 185 Countries. *CA. Cancer J. Clin.* **71**, 209–249 (2021).

2. Schadendorf, D. *et al.* Melanoma. *Lancet Lond. Engl.* **392**, 971–984 (2018).

3. De Pinto, G. *et al.* Global trends in cutaneous malignant melanoma incidence and mortality. *Melanoma Res.* **34**, 265–275 (2024).

4. Whiteman, D. C., Green, A. C. & Olsen, C. M. The Growing Burden of Invasive Melanoma: Projections of Incidence Rates and Numbers of New Cases in Six Susceptible Populations through 2031. *J. Invest. Dermatol.* **136**, 1161–1171 (2016).

5. Garbe, C. *et al.* European consensus-based interdisciplinary guideline for melanoma. Part 1: Diagnostics: Update 2022. *Eur. J. Cancer Oxf. Engl. 1990* **170**, 236–255 (2022).

6. Petty, A. J. *et al.* Meta-analysis of number needed to treat for diagnosis of melanoma by clinical setting. *J. Am. Acad. Dermatol.* **82**, 1158–1165 (2020).

7. Kibbie, J. J., Zita, S. M., Dellavalle, R. P., Dunnick, C. A. & Armstrong, C. A. The number needed to biopsy for cutaneous melanoma in academic dermatology clinics. *Melanoma Res.* **34**, 350–354 (2024).

8. van Dijk, M. C. R. F. *et al.* Expert review remains important in the histopathological diagnosis of cutaneous melanocytic lesions. *Histopathology* **52**, 139–146 (2008).

9. Urso, C., Saieva, C., Borgognoni, L., Tinacci, G. & Zini, E. Sensitivity and specificity of histological criteria in the diagnosis of conventional cutaneous melanoma. *Melanoma Res.* **18**, 253–258 (2008).

10. Bhoyrul, B. *et al.* Pathological review of primary cutaneous malignant melanoma by a specialist skin cancer multidisciplinary team improves patient care in the UK. *J. Clin. Pathol.* **72**, 482–486 (2019).

11. Hekler, A. *et al.* Pathologist-level classification of histopathological melanoma images with deep neural networks. *Eur. J. Cancer* **115**, 79–83 (2019).

12. Shoo, B. A., Sagebiel, R. W. & Kashani-Sabet, M. Discordance in the histopathologic diagnosis of melanoma at a melanoma referral center. *J. Am. Acad. Dermatol.* **62**, 751–756 (2010).

13. Brochez, L. *et al.* Inter-observer variation in the histopathological diagnosis of clinically suspicious pigmented skin lesions. *J. Pathol.* **196**, 459–466 (2002).

14. Hekler, A. *et al.* Deep learning outperformed 11 pathologists in the classification of histopathological melanoma images. *Eur. J. Cancer* **118**, 91–96 (2019).

15. Massi, D. *et al.* Impact of second opinion pathology review in the diagnosis and management of atypical melanocytic lesions: A prospective study of the Italian Melanoma Intergroup (IMI) and EORTC Melanoma Group. *Eur. J. Cancer Oxf. Engl. 1990* **189**, 112921 (2023).

16. Kittler, H. Evolution of the Clinical, Dermoscopic and Pathologic Diagnosis of Melanoma. *Dermatol. Pract. Concept.* **11**, e2021163S (2021).

17. Pusiol, T., Morichetti, D., Piscioli, F. & Zorzi, M. G. Theory and practical application of superficial atypical melanocytic proliferations of uncertain significance (SAMPUS) and melanocytic tumours of uncertain malignant potential (MELTUMP) terminology: experience with second opinion consultation. *Pathologica* **104**, 70–77 (2012).

18. Kerr, K. F. *et al.* Dermatopathologist Perceptions of Overdiagnosis of Melanocytic Skin Lesions and Association With Diagnostic Behaviors. *JAMA Dermatol.* **158**, 675–679 (2022).

19. Elder, D. E. *et al.* Diagnostic error, uncertainty, and overdiagnosis in melanoma. *Pathology (Phila.)* **55**, 206–213 (2023).

20. Elmore, J. G. *et al.* Pathologists' diagnosis of invasive melanoma and melanocytic proliferations: observer accuracy and reproducibility study. *BMJ* **357**, j2813 (2017).

21. Jartarkar, S. R. Artificial intelligence: Its role in dermatopathology. *Indian J. Dermatol. Venereol. Leprol.* **89**, 549–552 (2023).

22. Ackerman, L. V. Malignant melanoma of the skin; clinical and pathologic analysis of 75 cases. *Am. J. Clin. Pathol.* **18**, 602–624 (1948).

23. Allen, A. C. & Spitz, S. Malignant melanoma; a clinicopathological analysis of the criteria for diagnosis and prognosis. *Cancer* **6**, 1–45 (1953).

24. Breslow, A. Thickness, cross-sectional areas and depth of invasion in the prognosis of cutaneous melanoma. *Ann. Surg.* **172**, 902–908 (1970).

25. Massi, G. & LeBoit, P. E. *Histological Diagnosis of Nevi and Melanoma*. (Springer, Berlin, Heidelberg, 2014). doi:10.1007/978-3-642-37311-4.

26. Ackerman, A. B. An algorithmic method for histologic diagnosis of inflammatory and neoplastic skin diseases by analysis of their patterns. *Am. J. Dermatopathol.* **7**, 105–107 (1985).

27. Urso, C. *et al.* Interobserver reproducibility of histological features in cutaneous malignant melanoma. *J. Clin. Pathol.* **58**, 1194 (2005).

28. Bobos, M. Histopathologic classification and prognostic factors of melanoma: a 2021 update. *Ital. J. Dermatol. Venereol.* **156**, 300–321 (2021).

29. Piérard, G. E. Cell proliferation in cutaneous malignant melanoma: relationship with neoplastic progression. *ISRN Dermatol.* **2012**, 828146 (2012).

30. Abbas, O., Miller, D. D. & Bhawan, J. Cutaneous malignant melanoma: update on diagnostic and prognostic biomarkers. *Am. J. Dermatopathol.* **36**, 363–379 (2014).

31. Tuthill, R. J. *et al.* Risk assessment in localized primary cutaneous melanoma: a Southwest Oncology Group study evaluating nine factors and a test of the Clark logistic regression prediction model. *Am. J. Clin. Pathol.* **118**, 504–511 (2002).

32. van Houdt, I. S. *et al.* Favorable outcome in clinically stage II melanoma patients is associated with the presence of activated tumor infiltrating T-lymphocytes and preserved MHC class I antigen expression. *Int. J. Cancer* **123**, 609–615 (2008).

33. Compton, C. C., Barnhill, R., Wick, M. R., Balch, C., & Members of the Cancer Committee, College of American Pathologists. Protocol for the examination of specimens

from patients with melanoma of the skin. *Arch. Pathol. Lab. Med.* **127**, 1253–1262 (2003).

34. Aivazian, K. Regression in cutaneous melanoma: histological assessment, immune mechanisms and clinical implications. *Pathology (Phila.)* **55**, 227–235 (2023).

35. Abbas, O., Miller, D. D. & Bhawan, J. Cutaneous Malignant Melanoma: Update on Diagnostic and Prognostic Biomarkers. *Am. J. Dermatopathol.* **36**, 363–379 (2014).

36. Scolyer, R. A. *et al.* Data Set for Pathology Reporting of Cutaneous Invasive Melanoma: Recommendations From the International Collaboration on Cancer Reporting (ICCR). *Am. J. Surg. Pathol.* **37**, 1797–1814 (2013).

37. Bishop, J. & Tallon, B. Number of levels required to assess Breslow thickness in cutaneous invasive melanoma: An observational study. *J. Cutan. Pathol.* **46**, 819–822 (2019).

38. Kiehl, Matthies, Ehrich, Völker, & Kapp. Accuracy of frozen section measurements for the determination of Breslow tumour thickness in primary malignant melanoma. *Histopathology* **34**, 257–261 (1999).

39. Curti, N. *et al.* Breslow thickness: Geometric interpretation, potential pitfalls, and computer automated estimation. *Pathol. - Res. Pract.* **238**, 154117 (2022).

40. Rashed, H., Flatman, K., Bamford, M., Teo, K. W. & Saldanha, G. Breslow density is a novel prognostic feature in cutaneous malignant melanoma. *Histopathology* **70**, 264–272 (2017).

41. Urso, C., Saieva, C., Borgognoni, L., Tinacci, G. & Zini, E. Sensitivity and specificity of histological criteria in the diagnosis of conventional cutaneous melanoma. *Melanoma Res.* **18**, 253–258 (2008).

42. Löper, R., Schön, M. P. & Mitteldorf, C. Melanocyte Density in the Diagnosis of Melanoma In Situ in Sun-Damaged Skin. *Am. J. Dermatopathol.* **46**, 358–364 (2024).

43. Shitara, D. *et al.* Nevus-Associated Melanomas. *Am. J. Clin. Pathol.* **142**, 485–491 (2014).

44. Murali, R., Hughes, M. T., Fitzgerald, P., Thompson, J. F. & Scolyer, R. A. Interobserver Variation in the Histopathologic Reporting of Key Prognostic Parameters, Particularly Clark Level, Affects Pathologic Staging of Primary Cutaneous Melanoma. *Ann. Surg.* **249**, 641–647 (2009).

45. Drabeni, M. *et al.* Differences in Tumor Thickness Between Hematoxylin and Eosin and Melan-A Immunohistochemically Stained Primary Cutaneous Melanomas. *Am. J. Dermatopathol.* **35**, 56–63 (2013).

46. Palve, J. S., Ylitalo, L. K., Luukkaala, T. H., Jernman, J. M. & Korhonen, N. J. A second expert pathology review of cutaneous melanoma in multidisciplinary meetings: Impact on treatment decisions. *Surg. Oncol.* **30**, 72–75 (2019).

47. McDermott, N. C. *et al.* Identification of Vertical Growth Phase in Malignant Melanoma: A Study of Interobserver Agreement. *Am. J. Clin. Pathol.* **110**, 753–757 (1998).

48. Dixon, A. *et al.* Online prediction tools for melanoma survival: A comparison. *J. Eur. Acad. Dermatol. Venereol. JEADV* **37**, 1999–2003 (2023).

49. Chen, Y.-P. *et al.* PRAME is a useful marker for the differential diagnosis of melanocytic tumours and histological mimics. *Histopathology* **82**, 285–295 (2023).

50. Gosman, L. M., Țăpoi, D.-A. & Costache, M. Cutaneous Melanoma: A Review of Multifactorial Pathogenesis, Immunohistochemistry, and Emerging Biomarkers for Early Detection and Management. *Int. J. Mol. Sci.* **24**, 15881 (2023).

51. Dinehart, M. S., Dinehart, S. M., Sukpraprut-Braaten, S. & High, W. A. Immunohistochemistry utilization in the diagnosis of melanoma. *J. Cutan. Pathol.* **47**, 446–450 (2020).

52. Ferrara, G. & Argenziano, G. The WHO 2018 Classification of Cutaneous Melanocytic Neoplasms: Suggestions From Routine Practice. *Front. Oncol.* **11**, 675296 (2021).

53. Elder, D. E., Bastian, B. C., Cree, I. A., Massi, D. & Scolyer, R. A. The 2018 World Health Organization Classification of Cutaneous, Mucosal, and Uveal Melanoma: Detailed Analysis of 9 Distinct Subtypes Defined by Their Evolutionary Pathway. *Arch. Pathol. Lab. Med.* **144**, 500–522 (2020).

54. Lopez-Beltran, A., Canas-Marques, R., Cheng, L. & Montironi, R. Histopathologic challenges: The second OPINION issue. *Eur. J. Surg. Oncol. J. Eur. Soc. Surg. Oncol. Br. Assoc. Surg. Oncol.* **45**, 12–15 (2019).

55. Geller, B. M. *et al.* Pathologists' Use of Second Opinions in Interpretation of Melanocytic Cutaneous Lesions: Policies, Practices, and Perceptions. *Dermatol. Surg. Off. Publ. Am. Soc. Dermatol. Surg. Al* **44**, 177–185 (2018).

56. Piepkorn, M. W. *et al.* Assessment of Second-Opinion Strategies for Diagnoses of Cutaneous Melanocytic Lesions. *JAMA Netw. Open* **2**, e1912597 (2019).

57. Gaudi, S., Zarandona, J. M., Raab, S. S., English, J. C. & Jukic, D. M. Discrepancies in dermatopathology diagnoses: the role of second review policies and dermatopathology fellowship training. *J. Am. Acad. Dermatol.* **68**, 119–128 (2013).

58. Hawryluk, E. B. *et al.* Histologically challenging melanocytic tumors referred to a tertiary care pigmented lesion clinic. *J. Am. Acad. Dermatol.* **67**, 727–735 (2012).

59. Gibson, M. *et al.* Estimating the potential impact of interventions to reduce over-calling and under-calling of melanoma. *J. Eur. Acad. Dermatol. Venereol. JEADV* **35**, 1519–1527 (2021).

60. Ronen, S. *et al.* Discordance in Diagnosis of Melanocytic Lesions and Its Impact on Clinical Management. *Arch. Pathol. Lab. Med.* **145**, 1505–1515 (2021).

61. Lott, J. P. *et al.* Population-Based Analysis of Histologically Confirmed Melanocytic Proliferations Using Natural Language Processing. *JAMA Dermatol.* **154**, 24–29 (2018).

62. Cajal, S. R. y *et al.* Integrating clinical, molecular, proteomic and histopathological data within the tissue context: tissunomics. *Histopathology* **75**, 4 (2019).

63. Ricci, C. *et al.* Cutaneous Melanomas: A Single Center Experience on the Usage of Immunohistochemistry Applied for the Diagnosis. *Int. J. Mol. Sci.* **23**, 5911 (2022).

64. Dinehart, M. S., Dinehart, S. M., Sukpraprut-Braaten, S. & High, W. A. Immunohistochemistry utilization in the diagnosis of melanoma. *J. Cutan. Pathol.* **47**, 446–450 (2020).

65. Stiff, K. M., Franklin, M. J., Zhou, Y., Madabhushi, A. & Knackstedt, T. J. Artificial intelligence and melanoma: A comprehensive review of clinical, dermoscopic, and histologic applications. *Pigment Cell Melanoma Res.* **35**, 203–211 (2022).

66. Cazzato, G. *et al.* Artificial Intelligence Applied to a First Screening of Naevoid Melanoma: A New Use of Fast Random Forest Algorithm in Dermatopathology. *Curr. Oncol. Tor. Ont* **30**, 6066–6078 (2023).

67. Sauter, D. *et al.* Validating Automatic Concept-Based Explanations for AI-Based Digital Histopathology. *Sensors* **22**, 5346 (2022).

68. Potter, B. & Ronan, S. G. Computerized dermatopathologic diagnosis. *J. Am. Acad. Dermatol.* **17**, 119–131 (1987).

69. Feit, J., Kempf, W., Jedlicková, H. & Burg, G. Hypertext atlas of dermatopathology with expert system for epithelial tumors of the skin. *J. Cutan. Pathol.* **32**, 433–437 (2005).

70. Esteva, A. *et al.* Dermatologist-level classification of skin cancer with deep neural networks. *Nature* **542**, 115–118 (2017).

71. Hekler, A. *et al.* Pathologist-level classification of histopathological melanoma images with deep neural networks. *Eur. J. Cancer Oxf. Engl. 1990* **115**, 79–83 (2019).

72. Xie, P. *et al.* Interpretable Classification from Skin Cancer Histology Slides Using Deep Learning: A Retrospective Multicenter Study. Preprint at https://doi.org/10.48550/arXiv.1904.06156 (2019).

73. Brinker, T. J. *et al.* Diagnostic performance of artificial intelligence for histologic melanoma recognition compared to 18 international expert pathologists. *J. Am. Acad. Dermatol.* **86**, 640–642 (2022).

74. Cazzato, G. *et al.* Dermatopathology of Malignant Melanoma in the Era of Artificial Intelligence: A Single Institutional Experience. *Diagn. Basel Switz.* **12**, 1972 (2022).

75. Jiang, Y., Yang, M., Wang, S., Li, X. & Sun, Y. Emerging role of deep learning-based artificial intelligence in tumor pathology. *Cancer Commun. Lond. Engl.* **40**, 154–166 (2020).

76. Echle, A. *et al.* Deep learning in cancer pathology: a new generation of clinical biomarkers. *Br. J. Cancer* **124**, 686–696 (2021).

77. Salgado, R. & AbdulJabbar, K. Artificial intelligence biomarkers for digital oncology: a case study of tumor-infiltrating lymphocytes in melanoma. *eBioMedicine* **96**, (2023).

78. Sturm, B. *et al.* Computer-Aided Assessment of Melanocytic Lesions by Means of a Mitosis Algorithm. *Diagn. Basel Switz.* **12**, 436 (2022).

79. Kulkarni, P. M. *et al.* Deep Learning Based on Standard H&E Images of Primary Melanoma Tumors Identifies Patients at Risk for Visceral Recurrence and Death. *Clin. Cancer Res. Off. J. Am. Assoc. Cancer Res.* **26**, 1126–1134 (2020).

80. Mosquera-Zamudio, A. *et al.* Deep Learning for Skin Melanocytic Tumors in Whole-Slide Images: A Systematic Review. *Cancers* **15**, 42 (2022).

81. Cazzato, G. & Rongioletti, F. Artificial intelligence in dermatopathology: Updates, strengths, and challenges. *Clin. Dermatol.* **42**, 437–442 (2024).

82. Stiff, K. M., Franklin, M. J., Zhou, Y., Madabhushi, A. & Knackstedt, T. J. Artificial intelligence and melanoma: A comprehensive review of clinical, dermoscopic, and histologic applications. *Pigment Cell Melanoma Res.* **35**, 203–211 (2022).

83. Otsu, N. A Threshold Selection Method from Gray-Level Histograms. *IEEE Trans. Syst. Man Cybern.* **9**, 62–66 (1979).

84. Ronneberger, O., Fischer, P. & Brox, T. U-Net: Convolutional Networks for Biomedical Image Segmentation. Preprint at https://doi.org/10.48550/arXiv.1505.04597 (2015).

85. Gamper, J. *et al.* PanNuke Dataset Extension, Insights and Baselines. Preprint at https://doi.org/10.48550/arXiv.2003.10778 (2020).

86. Goode, A., Gilbert, B., Harkes, J., Jukic, D. & Satyanarayanan, M. OpenSlide: A vendor-neutral software foundation for digital pathology. *J. Pathol. Inform.* **4**, 27 (2013).

87. Ooms [aut, J., cre & Wijffels, J. opencv: Bindings to 'OpenCV' Computer Vision Library. (2024).

88. Martel, A. *et al.* An Image Analysis Resource for Cancer Research: PIIP—Pathology Image Informatics Platform for Visualization, Analysis, and Management. *Cancer Res.* **77**, e83–e86 (2017).

89. Mooi, W. J. & Krausz, T. The Histological Diagnosis of Cutaneous Melanoma. in *Diagnosis and Management of Melanoma in Clinical Practice* (eds. Kirkham, N., Cotton,

D. W. K., Lallemand, R. C., White, J. E. & Rosin, R. D.) 61–73 (Springer, London, 1992). doi:10.1007/978-1-4471-1925-8_6.

90. Nawaz, S. & Yuan, Y. Computational pathology: Exploring the spatial dimension of tumor ecology. *Cancer Lett.* **380**, 296–303 (2016).

91. Bull, J. A. *et al.* Combining multiple spatial statistics enhances the description of immune cell localisation within tumours. *Sci. Rep.* **10**, 18624 (2020).

92. Nguyen, L. *et al.* Spatial Statistics for Segmenting Histological Structures in H&E Stained Tissue Images. *IEEE Trans. Med. Imaging* **36**, 1522–1532 (2017).

93. Gupta, R., Kurc, T., Sharma, A., Almeida, J. S. & Saltz, J. The Emergence of Pathomics. *Curr. Pathobiol. Rep.* **7**, 73–84 (2019).

94. van Zon, M. *et al.* Segmentation and Classification of Melanoma and Nevus in Whole Slide Images. in *2020 IEEE 17th International Symposium on Biomedical Imaging (ISBI)* 263–266 (2020). doi:10.1109/ISBI45749.2020.9098487.

95. Martel, A. L. *et al.* An Image Analysis Resource for Cancer Research: PIIP-Pathology Image Informatics Platform for Visualization, Analysis, and Management. *Cancer Res.* **77**, e83–e86 (2017).

96. Dall'Olio, D. *et al.* Impact of concurrency on the performance of a whole exome sequencing pipeline. *BMC Bioinformatics* **22**, 60 (2021).

97. Haralick, R. M., Shanmugam, K. & Dinstein, I. Textural Features for Image Classification. *IEEE Trans. Syst. Man Cybern.* **SMC-3**, 610–621 (1973).

98. Hahsler, M., Piekenbrock, M. & Doran, D. dbscan: Fast Density-Based Clustering with R. *J. Stat. Softw.* **91**, 1–30 (2019).

99. Diggle, P. J., Tawn, J. A. & Moyeed, R. A. Model-Based Geostatistics. *J. R. Stat. Soc. Ser. C Appl. Stat.* **47**, 299–350 (1998).

100. Gräler, B., Pebesma, E. & Heuvelink, G. Spatio-Temporal Interpolation using gstat. *R J.* **8**, 204–218 (2016).

101. Baddeley, A. & Turner, R. spatstat: An R Package for Analyzing Spatial Point Patterns. *J. Stat. Softw.* **12**, 1–42 (2005).

102. Hastie, T., Tibshirani, R. & Friedman, J. *The Elements of Statistical Learning*. (Springer, New York, NY, 2009). doi:10.1007/978-0-387-84858-7.

103. Friedman, J. H. Regularized Discriminant Analysis. *J. Am. Stat. Assoc.* **84**, 165–175 (1989).

104. Venables, W. N. & Ripley, B. D. *Modern Applied Statistics with S*. (Springer, New York, NY, 2002). doi:10.1007/978-0-387-21706-2.

105. Weihs, C., Ligges, U., Luebke, K. & Raabe, N. klaR Analyzing German Business Cycles. in *Data Analysis and Decision Support* (eds. Baier, D., Decker, R. & Schmidt-

Thieme, L.) 335–343 (Springer, Berlin, Heidelberg, 2005). doi:10.1007/3-540-28397-8_36.

106. Martel, A. L. *et al.* An Image Analysis Resource for Cancer Research: PIIP—Pathology Image Informatics Platform for Visualization, Analysis, and Management. *Cancer Res.* **77**, e83–e86 (2017).

107. Balch, C. M. *et al.* Final Version of 2009 AJCC Melanoma Staging and Classification. *J. Clin. Oncol.* **27**, 6199–6206 (2009).

108. Dixon, A. *et al.* Online prediction tools for melanoma survival: A comparison. *J. Eur. Acad. Dermatol. Venereol.* **37**, 1999–2003 (2023).

109. Walker, R. J. B. *et al.* Predictors of Sentinel Lymph Node Metastasis in Patients with Thin Melanoma: An International Multi-institutional Collaboration. *Ann. Surg. Oncol.* **29**, 7010–7017 (2022).

110. on behalf of the Italian Melanoma Intergroup (IMI) *et al.* Clinicopathological predictors of recurrence in nodular and superficial spreading cutaneous melanoma: a multivariate analysis of 214 cases. *J. Transl. Med.* **15**, 227 (2017).

111. Ribero, S., Quaglino, P. & Roccuzzo, G. Predicting progression in very thin melanoma: the challenge of the next decade? *Br. J. Dermatol.* **189**, 362–363 (2023).

112. Richetta, A. G. *et al.* Thin melanoma and late recurrences: it is never too thin and never too late. *Med. Oncol.* **31**, 909 (2014).

113. Valentini, V. *et al.* MiRNAs as Potential Prognostic Biomarkers for Metastasis in Thin and Thick Primary Cutaneous Melanomas. *Anticancer Res.* **39**, 4085–4093 (2019).

114. Dessinioti, C. *et al.* A Retrospective Study of Diameter and Breslow Thickness in Invasive Melanomas. *Dermatology* 1–6 (2024) doi:10.1159/000536151.

115. Jaeger, J. *et al.* Gene Expression Signatures for Tumor Progression, Tumor Subtype, and Tumor Thickness in Laser-Microdissected Melanoma Tissues. *Clin. Cancer Res.* **13**, 806–815 (2007).

116. Dika, E. *et al.* Defining the Prognostic Role of MicroRNAs in Cutaneous Melanoma. *J. Invest. Dermatol.* **140**, 2260–2267 (2020).

117. Glud, M. & Gniadecki, R. MicroRNAs in the pathogenesis of malignant melanoma. *J. Eur. Acad. Dermatol. Venereol.* **27**, 142–150 (2013).

118. Cadby, G. *et al.* The association of host and genetic melanoma risk factors with Breslow thickness in the Western Australian Melanoma Health Study. *Br. J. Dermatol.* **170**, 851–857 (2014).

119. Rodriguez, M., Aladowicz, E., Lanfrancone, L. & Goding, C. R. Tbx3 Represses E-Cadherin Expression and Enhances Melanoma Invasiveness. *Cancer Res.* **68**, 7872–7881 (2008).

120. Kumar, S. *et al.* A Pathway for the Control of Anoikis Sensitivity by E-Cadherin and Epithelial-to-Mesenchymal Transition. *Mol. Cell. Biol.* **31**, 4036–4051 (2011).

121. Lade-Keller, J. *et al.* E- to N-cadherin switch in melanoma is associated with decreased expression of phosphatase and tensin homolog and cancer progression. *Br. J. Dermatol.* **169**, 618–628 (2013).

122. Lobos-González, L. *et al.* E-cadherin determines C aveolin-1 tumor suppression or metastasis enhancing function in melanoma cells. *Pigment Cell Melanoma Res.* **26**, 555–570 (2013).

123. Van Kempen, L. C., Redpath, M., Robert, C. & Spatz, A. Molecular pathology of cutaneous melanoma. *Melanoma Manag.* **1**, 151–164 (2014).

Elenco pubblicazioni

Durante il periodo di Dottorato sono state prodotte le seguenti pubblicazioni.

1) Lentigo Maligna and Lentigo Maligna Melanoma of the External Ear: Clinical and Dermoscopic Features of 19 Patients. Dika E, Venturi F, Veronesi G, Veneziano L, Scotti B.Exp Dermatol. 2024 Oct;33(10):e15188. doi: 10.1111/exd.15188.PMID: 39367572

2) Amelanotic melanoma of the nail unit: Clinical and dermoscopic features of the nail plate changes. Dika E, Fanti PA, Baraldi C, Venturi F, Scotti B, Veronesi G, Miccio L, Vaccari S.Skin Res Technol. 2024 Sep;30(9):e70051. doi: 10.1111/srt.70051.PMID: 39258794

3) Basosquamous carcinoma: Comprehensive epidemiological, clinical, dermoscopic, and confocal features from a single center institution. Venturi F, Erbacci V, Veronesi G, Scotti B, Baraldi C, Dika E.Skin Res Technol. 2024 Aug;30(8):e70012. doi: 10.1111/srt.70012.PMID: 39137046

4) Reflectance confocal microscopy and dermoscopic features of acrodermatitis continua of Hallopeau. Venturi F, Alessandrini A, Veronesi G, Baraldi C, Dika E.Int J Dermatol. 2024 Aug 9. doi: 10.1111/ijd.17433. Online ahead of print.PMID: 39123280

5) Reflectance confocal microscopy as noninvasive tool for monitoring tirbanibulin efficacy in actinic keratosis. Venturi F, Veronesi G, Baraldi C, Dika E.Photodiagnosis Photodyn Ther. 2024 Aug;48:104235. doi: 10.1016/j.pdpdt.2024.104235. Epub 2024 Jun 6.PMID: 38851311

6) Clinic and dermoscopy of genital basal cell carcinomas (gBCCs): a retrospective analysis among 169 patients referred with genital skin neoplasms. Scotti B, Vaccari S, Maltoni L, Robuffo S, Veronesi G, Dika E.Arch Dermatol Res. 2024 May 31;316(6):307. doi: 10.1007/s00403-024-03068-z.PMID: 38819453

7) A Nodular Melanoma Mimicking a Blue Nevus: A Case Report. D'Agostino GM, Bianchelli T, Veronesi G, Di Gregorio V, Brancorsini D.Dermatol Pract Concept. 2024 Apr 1;14(2):e2024116. doi: 10.5826/dpc.1402a116.PMID: 38810052

8) A Comparative Demographic Study of Atypical Spitz Nevi and Malignant Melanoma. Dika E, Lambertini M, Venturi F, Veronesi G, Mastroeni S, Hrvatin Stancic B, Bergant-Suhodolcan A.Acta Dermatovenerol Croat. 2023 Dec;31(3):165-168.PMID: 38439731

9) Reflectance confocal microscopy features of chronic radiodermatitis: A useful tool for presurgical mapping. Rapparini L, Venturi F, Gelati C, Giorgini F, Pignatti M, Placa M, Scotti B, Veronesi G, Dika E.Skin Res Technol. 2024 Feb;30(2):e13621. doi: 10.1111/srt.13621.PMID: 38391115

10) Onychopapilloma: does free edge confocal microscopy of the nail improve the diagnosis?Veronesi G, Scotti B, Vaccari S, Baraldi C, Magnaterra E, Dika E.Skin Res Technol. 2024 Feb;30(2):e13592. doi: 10.1111/srt.13592.PMID: 38282281

11) Lentigo maligna (LM) of the auricular concha: Confocal microscopy and dermoscopy. Dika E, Scotti B, Alessandrini A, Veronesi G.Skin Res Technol. 2024 Jan;30(1):e13557. doi: 10.1111/srt.13557.PMID: 38186059

12) Canaliculitis mimicking cutaneous squamous cell carcinoma of the palpebral rim: A case report. Vaccari S, Roda M, Grendele A, Cassini F, Robuffo S, Veronesi G, Venturi F, Balbi T, Dika E.J Eur Acad Dermatol Venereol. 2024 Jul;38(7):e584-e586. doi: 10.1111/jdv.19757. Epub 2023 Dec 18.PMID: 38108524

13) Depicting dermoscopic and confocal findings in patients with Gorlin-Goltz Syndrome. Dika E, Lambertini M, Veronesi G, Misciali C, Ricci C, Longo C.Ital J Dermatol Venerol. 2023 Dec;158(6):500-501. doi: 10.23736/S2784-8671.23.07623-5.PMID: 38015487

14) Basic Elements of Artificial Intelligence Tools in the Diagnosis of Cutaneous Melanoma. Querzoli G, Veronesi G, Corti B, Nottegar A, Dika E.Crit Rev Oncog. 2023;28(3):37-41. doi: 10.1615/CritRevOncog.2023050220.PMID: 37968992

15) Unusual presentation of porokeratotic lichen planus: Histology, dermoscopy and confocal microscopy imaging of a rare condition. Scotti B, Veronesi G, Misciali C, Venturi F, Dika E.Skin Res Technol. 2023 Nov;29(11):e13521. doi: 10.1111/srt.13521.PMID: 37937416

16) The role of confocal microscopy in recurrent cutaneous angiosarcoma. Rossi AN, Veronesi G, Dika E.Skin Res Technol. 2023 Aug;29(8):e13423. doi: 10.1111/srt.13423.PMID: 37632190

17) Reflectance confocal microscopy of large penis pigmentation: A clue for detection of genital melanosis. Dika E, Venturi F, Veronesi G.Skin Res Technol. 2023 May;29(5):e13347. doi: 10.1111/srt.13347.PMID: 37231933

18) Follicular colonization in melanocytic nevi and melanoma: A literature review. Lambertini M, Ricci C, Corti B, Veronesi G, Quaglino P, Ribero S, Pellacani G, Hrvatin Stancic B, Campione E, Dika E.J Cutan Pathol. 2023 Aug;50(8):773-778. doi: 10.1111/cup.14415. Epub 2023 Mar 12.PMID: 36820529 Review.

19) Multiple primary melanomas: Is there a correlation between dermoscopic features and germline mutations? Lambertini M, Zengarini C, Ravaioli GM, Veronesi G, Mussi M, Ferrari T, Braschi G, Campione E, Dika E.Australas J Dermatol. 2023 May;64(2):e182-e185. doi: 10.1111/ajd.14007. Epub 2023 Feb 12.PMID: 36774630

20) Breslow thickness: Geometric interpretation, potential pitfalls, and computer automated estimation. Curti N, Veronesi G, Dika E, Misciali C, Marcelli E, Giampieri E.Pathol Res Pract. 2022 Oct;238:154117. doi: 10.1016/j.prp.2022.154117. Epub 2022 Sep 5.PMID: 36126452

21) Advantages of manual and automatic computer-aided compared to traditional histopathological diagnosis of melanoma: A pilot study. Dika E, Curti N, Giampieri E, Veronesi G, Misciali C, Ricci C, Castellani G, Patrizi A, Marcelli E.Pathol Res Pract.

2022 Sep;237:154014. doi: 10.1016/j.prp.2022.154014. Epub 2022 Jul 8.PMID: 35870238

22) Cutaneous Melanomas: A Single Center Experience on the Usage of Immunohistochemistry Applied for the Diagnosis. Ricci C, Dika E, Ambrosi F, Lambertini M, Veronesi G, Barbara C.Int J Mol Sci. 2022 May 25;23(11):5911. doi: 10.3390/ijms23115911.PMID: 35682589

23) Dysplastic nevi and melanoma: microRNAs tell a divergent story. Durante G, Veronesi G, Misciali C, Riefolo M, Lambertini M, Tartari F, Ricci C, Ferracin M, Dika E.Pathol Res Pract. 2022 Jul;235:153942. doi: 10.1016/j.prp.2022.153942. Epub 2022 May 14.PMID: 35594599

24) Female melanoma and estrogen receptors expression: an immunohistochemical pilot study. Dika E, Lambertini M, Lauriola M, Veronesi G, Ricci C, Tartari F, Tassone D, Campione E, Scarfì F.Melanoma Res. 2022 Aug 1;32(4):231-240. doi: 10.1097/CMR.0000000000000826. Epub 2022 May 13.PMID: 35579670

25) Hematoxylin and eosin or double stain for CD34/SOX10: Which is better for the detection of lymphovascular invasion in cutaneous melanoma? Ricci C, Dika E, Lambertini M, Ambrosi F, Grillini M, Chillotti S, Corradini AG, Veronesi G, Fiorentino M, Corti B.Pathol Res Pract. 2022 May;233:153876. doi: 10.1016/j.prp.2022.153876. Epub 2022 Apr 1.PMID: 35390633

26) The EORTC protocol for sentinel lymph node biopsy (SLNB) reveals a high number of nodal nevi and a strong association with nevus-associated melanoma. Ricci C, Dika E, Lambertini M, Ambrosi F, Chiarucci F, Chillotti S, Fiorentino M, Fabbri E, Tassone D, Veronesi G, Tartari F, Corti B.Pathol Res Pract. 2022 May;233:153805. doi: 10.1016/j.prp.2022.153805. Epub 2022 Mar 28.PMID: 35361504

27) BRAF V600K vs. BRAF V600E: a comparison of clinical and dermoscopic characteristics and response to immunotherapies and targeted therapies. Zengarini C, Mussi M, Veronesi G, Alessandrini A, Lambertini M, Dika E.Clin Exp Dermatol. 2022 Jun;47(6):1131-1136. doi: 10.1111/ced.15113. Epub 2022 Mar 11.PMID

28) Biological therapy in patients with psoriasis: What we know about the effects on renal function. Veronesi G, Guglielmo A, Gardini A, Sacchelli L, Loi C, Patrizi A, Bardazzi F.Dermatol Ther. 2022 Jan;35(1):e15202. doi: 10.1111/dth.15202. Epub 2021 Nov 24.PMID: 34773435

29) Vulvar vitiligo and lichen sclerosus in children: A clinical challenge. Veronesi G, Virdi A, Leuzzi M, Gurioli C, Chessa MA, Guglielmo A, Neri I.Pediatr Dermatol. 2021 Sep;38(5):1012-1019. doi: 10.1111/pde.14771. Epub 2021 Sep 24. PMID: 34561885 Review.

30) An Unusual Case of Meyerson Phenomenon Around Infantile Hemangioma. Veronesi G, Leuzzi M, Virdi A, Gurioli C, Neri I.Dermatol Pract Concept. 2021 Jul 8;11(3):e2021039. doi: 10.5826/dpc.1103a39. eCollection 2021 Jul.PMID: 34414001.

31) Basaloid follicular hamartomas in pediatric Basal Cell Nevus Syndrome: A diagnostic challenge. Besagni F, Dika E, Ricci C, Misciali C, Veronesi G, Corti B, Gurioli C, Neri I.J Dermatol. 2021 Jul;48(7):1101-1105. doi: 10.1111/1346-8138.15892. Epub 2021 May 21.PMID: 34021633

32) Post-traumatic panniculitis: skin sign of torture. Magnano M, Veronesi G, Baraldi C, Chessa MA, Patrizi A, Bardazzi F.Ital J Dermatol Venerol. 2022 Feb;157(1):105-106. doi: 10.23736/S2784-8671.21.06868-7. Epub 2021 Apr 23.PMID: 33890731